



Cite this: *Phys. Chem. Chem. Phys.*, 2021, 23, 19964

## Breakdown of the Stokes–Einstein relation in supercooled water: the jump-diffusion perspective†

Vikas Dubey, Shivam Dueby and Snehasis Daschakraborty \*

Although water is the most ubiquitous liquid it shows many thermodynamic and dynamic anomalies. Some of the anomalies further intensify in the supercooled regime. While many experimental and theoretical studies have focused on the thermodynamic anomalies of supercooled water, fewer studies explored the dynamical anomalies very extensively. This is due to the intricacy of the experimental measurement of the dynamical properties of supercooled water. Violation of the Stokes–Einstein relation (SER), an important relation connecting the diffusion of particles with the viscosity of the medium, is one of the major dynamical anomalies. In absence of experimentally measured viscosity, researchers used to check the validity of SER indirectly using average translational relaxation time or  $\alpha$ -relaxation time. Very recently, the viscosity of supercooled water was accurately measured at a wide range of temperatures and pressures. This allowed direct verification of the SER at different temperature-pressure thermodynamic state points. An increasing breakdown of the SER was observed with decreasing temperature. Increasing pressure reduces the extent of breakdown. Although some well-known theories explained the above breakdown, a detailed molecular mechanism was still elusive. Recently, a translational jump-diffusion (TJD) approach has been able to quantitatively explain the breakdown of the SER in pure supercooled water and an aqueous solution of methanol. The objective of this article is to present a detailed and state-of-the-art analysis of the past and present works on the breakdown of SER in supercooled water with a specific focus on the new TJD approach for explaining the breakdown of the SER.

Received 18th May 2021,  
Accepted 6th September 2021

DOI: 10.1039/d1cp02202d

rsc.li/pccp

Department of Chemistry, Indian Institute of Technology Patna, Bihar 801106, India. E-mail: [snehasis@iitp.ac.in](mailto:snehasis@iitp.ac.in)

† Electronic supplementary information (ESI) available: Simulated and experimental transport properties, which are fitted with VFT and power law. See DOI: [10.1039/d1cp02202d](https://doi.org/10.1039/d1cp02202d)



Vikas Dubey

*Vikas Dubey completed his MSc in Chemistry from C.S.J.M. University, Kanpur, India. He joined the Department of Chemistry, Indian Institute of Technology Patna, India in 2017 as a Junior Research Fellow under the supervision of Dr Snehasis Daschakraborty. Currently, he is a Senior Research Fellow (SRF). His research interests mainly focused on the role of translational jump-diffusion in supercooled water and other related systems.*



Shivam Dueby

*Shivam Dueby completed his MSc in Chemistry from Aligarh Muslim University, India. He joined the Department of Chemistry, Indian Institute of Technology Patna, India in 2018 as a Junior Research Fellow under the supervision of Dr Snehasis Daschakraborty. Currently, he is a Senior Research Fellow (SRF). His research interest is mainly focused on the dynamics of glass-forming liquids.*

common liquid, water shows many anomalous behaviors, some of which further intensify on cooling below freezing point and attaining the supercooled regime.<sup>1–15</sup> Occurrence of the density maximum at 4 °C and rapid variation of different thermodynamic response functions, such as isothermal compressibility, thermal expansion coefficient, heat capacity, *etc.* with decreasing temperature are some of the thermodynamic anomalies of supercooled water. Since liquid water remains thermodynamically less stable than ice in the supercooled regime, it is difficult to perform experiments on supercooled water. However, with the advancement of experimental techniques, it has been possible to perform various experiments in supercooled water and provide new insights.

Many researchers investigated the origin of the thermodynamic anomalies in supercooled water over the last few decades.<sup>5–7,16–23</sup> Different theories were proposed to explain the anomalies.<sup>16,24–33</sup> One of the first approaches was the “stability-limit conjecture” (SLC),<sup>34–36</sup> which aimed at explaining the anomalies by presenting a unified thermodynamic understanding. The SLC approach proposed that unlike in simple liquid, where the liquid spinodal (emerging from the liquid–vapor critical point) continues to decrease steadily into the negative pressure region with decreasing temperature in a temperature–pressure (*T*–*P*) phase diagram, the liquid spinodal for supercooled water returns to positive pressure after it intersects the “temperature of maximum density” (TMD) line. The divergence of fluctuations at the spinodal can explain the rapid increase of the thermodynamic response functions upon cooling. Another proposed explanation is the liquid–liquid critical point (LLCP) hypothesis, in which the anomalous properties of supercooled water are explained in terms of the first-order liquid–liquid

phase transitions.<sup>16,17,24,30,31,37–40</sup> Below the LLCP temperature there exists two distinct phases of water: low-density liquid (LDL) and high-density liquid (HDL). Beyond the LLCP these two states become indistinguishable. In another two-state model picture, water was assumed to be a mixture of two inter-convertible states: low-density state (LDS) and high-density state (HDS).<sup>41–45</sup> The singularity-free approach (SFA)<sup>32</sup> and the critical-point-free (CPF)<sup>33,46</sup> approaches were also utilized to explain some anomalies of supercooled water. While the CPF approach is an alternative form of the LLCP hypothesis with the critical point at large negative pressure, the SFA scenario is distinguished by the sharp but nondivergent maxima in the response functions at different temperatures. In the SFA scenario, there is no liquid–liquid transition.<sup>47</sup>

Unlike the thermodynamic anomalies, the dynamic anomalies were not extensively studied in experiments. This is because of the intricacy of performing experiments revealing the dynamics of supercooled water. However, recent experiments have been probing dynamical anomalies, such as increasing diffusion and decreasing viscosity under compression,<sup>48</sup> crossover from fragile-to-strong liquid dynamics,<sup>48–53</sup> and earlier decoupling of self-diffusion from viscosity upon cooling.<sup>54</sup> Although it is being quite a while since the self-diffusion coefficient, the rotational and translational relaxation times were measured at different *T*–*P* state points, quantitative estimation of the viscosity coefficient was done only recently.<sup>48</sup> The viscosity of supercooled water was measured down to 239 K temperature and up to 300 MPa pressure. At a given temperature, the viscosity starts decreasing with increasing pressure, reaches a minimum, and then increases. While at ambient temperature the minimum is rather shallow, the depth increases with decreasing temperature. An extension of the two-state model,<sup>45</sup> which explained the thermodynamic anomalies, was able to describe the dynamical properties: self-diffusion, viscosity, and rotational correlation time accurately at different *T*–*P* state points.<sup>48</sup> This also explained the dynamical crossover from fragile-to-strong liquid behavior in a reasonable accuracy.

The presence of accurate measurement of viscosity and self-diffusion coefficients of supercooled water at different *T*–*P* state points allows checking the validity of the Stokes–Einstein relation (SER), an important relationship for understanding the nature of molecular diffusion in liquid.<sup>48,54</sup> Since the SER was derived from Einstein’s theory of Brownian motion, it assumes the applicability of Einstein’s model of diffusion. The absence of accurate viscosity coefficients restricted researchers to verify the SER by studying the coupling between the average translational relaxation time and the self-diffusion coefficient of supercooled water.<sup>55–61</sup> This is an indirect way of checking the validity of SER. The direct verification has been performed relatively recently with the accurately measured viscosities at different *T*–*P* state points.<sup>48,54</sup> Several computer simulation studies have also focused on the validity of the SER in supercooled water and provided deep molecular insights into it.<sup>62,63</sup> The existing theories for explaining the thermodynamic anomalies of supercooled water were modified and



**Snehasis Daschakraborty**

*Snehasis Daschakraborty is an Assistant Professor in the Department of Chemistry, Indian Institute of Technology Patna, India. He received his PhD from the S. N. Bose National Center for Basic Sciences (Jadavpur University), Kolkata in 2014. His broad area of research is on the molecular dynamics of liquids and biomolecules. He has been working on topics like the breakdown of the Stokes–Einstein relation in supercooled water,*

*adaptation of cell membrane in extremophiles, permeation of nanoparticles across a lipid membrane, hydrophobic interaction in supercooled water, etc. He was a recipient of the INSA Medal for the Young Scientists Award 2020 for his works in the dynamics of supercooled water. He has been elected as a member of The National Academy of Science, India (M. N. A. Sc.) in 2021. Other details about his research group can be found at <https://www.sdmdlab-iitp.com/>.*

used to explain the dynamic anomalies.<sup>48</sup> Although these theories explained the above breakdown, a detailed molecular mechanism was still elusive. Recently, our group has been able to explain quantitatively the breakdown of SER using the translational jump-diffusion (TJD) approach.<sup>64–66</sup> In this approach, the translational jump-diffusion coefficient, which emanates from the translational jump (large amplitude displacement) of the molecules and contributes a part of the total diffusion, is calculated using a quantitative fashion. Interestingly, the remaining part of the diffusion stays coupled to the viscosity of the medium reasonably strongly in the supercooled water.

The objective of this article is to present a detailed and state-of-the-art analysis of the breakdown of SER in supercooled water. Since a vast literature is present on the same topic in supercooled liquid in general, this perspective is limited to supercooled water. Following is the organization of the remainder of this article. The origin of SER is detailed in Section 2. Section 3 summarizes the findings of prior studies focusing on the validity of SER in supercooled water. In Section 4 we have presented the TJD approach and its application in some systems to explain the breakdown of SER. The concluding remarks and the future scope are presented in Section 5.

## 2. The derivation and approximations of the SER

The derivation of SER was presented earlier.<sup>67–70</sup> Here, we summarize the key steps and approximations involved. The differential form of Einstein's diffusion equation for the translational motion of a Brownian particle can be written as,

$$\frac{\partial \rho(\mathbf{r}, t)}{\partial t} = D \frac{\partial^2 \rho(\mathbf{r}, t)}{\partial r^2} \quad (1)$$

The above equation comes from the combination of Fick's law of diffusion and the continuity equation. Here,  $\rho(\mathbf{r}, t)$  is the position ( $\mathbf{r}$ ) and time ( $t$ )-dependent density and  $D$  is the self-diffusion coefficient of the Brownian particle.  $\rho(\mathbf{r}, t)$  is solved to obtain the following expression for the motion in three dimensions,

$$\rho(\mathbf{r}, t) = \frac{1}{(4\pi D t)^{3/2}} e^{-|\mathbf{r}|^2/4Dt} \quad (2)$$

Eqn (2) can be used to calculate the mean square displacement (MSD)  $\langle r^2(t) \rangle = 6Dt$ , where “ $\langle \rangle$ ” symbols represent ensemble average. Eqn (2) shows how the density distribution in space changes with time. The Gaussian nature of  $\rho(\mathbf{r}, t)$  as a function of position  $\mathbf{r}$  at a given time  $t$  comes from the stochastic approximation. Now, we write the Langevin equation,

$$m\mathbf{r} + \xi\dot{\mathbf{r}} = \mathbf{F}(t) \quad (3)$$

where  $m$  is the mass of the particle,  $\xi$  is the frictional coefficient, and  $\mathbf{F}(t)$  is the random force that originates from the continuous collision of the Brownian particle with neighboring solvent particles.  $\mathbf{F}(t)$  has the following characteristics: (i)  $\mathbf{F}(t)$  is independent of velocity and the time-averaged value is zero  $\langle \mathbf{F}(t) \rangle = 0$ , and (ii)  $\mathbf{F}(t)$  varies faster in comparison to the velocity

of the particles. Solving eqn (3) for  $\langle r^2(t) \rangle$  and using the Einstein's equation at long time limit,  $\langle r^2(t) \rangle = 6Dt$  (for diffusion in three dimensions), one obtains,

$$D = \frac{k_B T}{\xi} \quad (4)$$

In eqn (4),  $\xi$  is assumed to be the friction on a spherical object of radius  $R$  with a stick hydrodynamic condition. Stokes law of friction provides the following equation for  $\xi$ :

$$\xi = 6\pi\eta R \quad (5)$$

In eqn (5),  $\eta$  is the viscosity of the medium. From eqn (4) and (5), we get the following expression of the SER,

$$D = k_B T / 6\pi\eta R \quad (6)$$

For the diffusion of a Brownian particle, the above SER is also written as

$$D \propto T/\eta \text{ or } D\eta/T = \text{constant} \quad (7)$$

The unavailability of accurate viscosity data does not allow using eqn (7). Instead, the average translational relaxation time  $\langle \tau_T \rangle$  or the  $\alpha$ -relaxation time  $\tau_\alpha$  is used to indirectly check the validity of SER by checking the constancy of  $(D\tau_T/T)$  or  $(D\tau_\alpha/T)$  with respect to temperature. This is based on the assumption that both  $\langle \tau_T \rangle$  and  $\tau_\alpha$  are linearly proportional to  $\eta$ . We will come back to this point in Section 3.2.

We now summarize the key approximations involved in the derivation of SER. A clear idea about the approximations would help in figuring out the cause of the breakdown of SER. (i) Stokes' law of friction is a hydrodynamic law that is applicable for diffusing particles much larger compared to solvent particles. (ii) The medium is structurally and dynamically homogenous to maintain the continuum nature. For example, the local viscosity, experienced by the diffusing particle, should be the same as the overall viscosity of the medium. (iii) In each step, the diffusing particles translate by a small distance. (iv) The trajectories of diffusing particles are uncorrelated and stochastic over long times. These assumptions principally restrict the usage of the SER in real scenarios. However, SER remains valid in many systems where such approximation(s) do not fully hold. There are a large number of systems where the severe breakdown of SER is observed. Supercooled water is one of them. Many experimental and simulation studies observed the breakdown in supercooled water and investigated the possible mechanism. We review these studies in the next section.

## 3. Verification of the SER in supercooled water and explanations

### 3.1 Indirect verification of SER

In this section, we will review studies that focused on the verification of SER by checking the constancy of  $(D\tau_T/T)$  or  $(D\tau_\alpha/T)$  with respect to temperature in the absence of viscosity data. Chen *et al.*<sup>55</sup> reported the translational self-diffusion

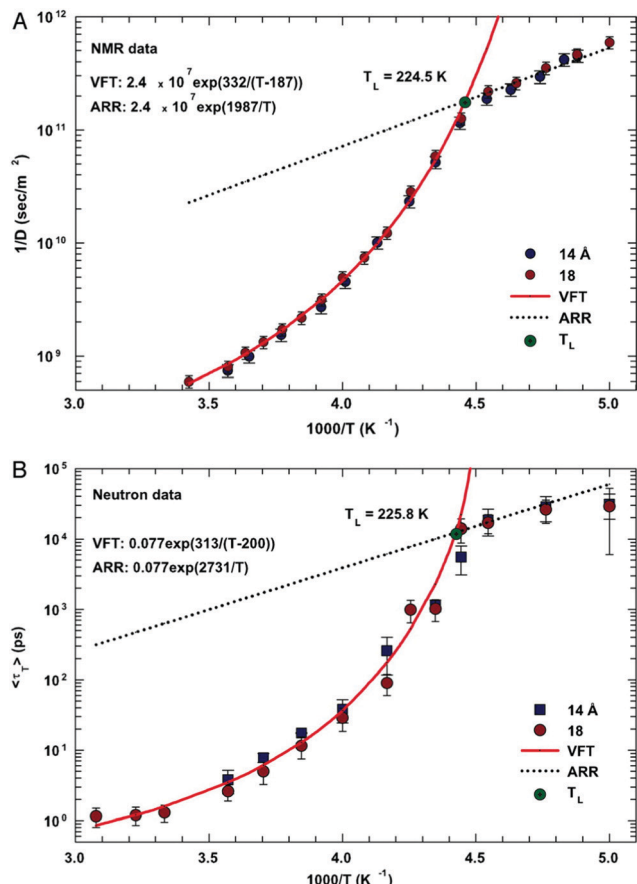


Fig. 1 The temperature dependence of the inverse of self-diffusion coefficient of water and its average translational relaxation time. (A) For the fully hydrated MCM-41-S samples with diameters of  $14$  and  $18 \text{ \AA}$ , the inverse of the self-diffusion coefficient of water  $D$  was measured by NMR as a function of  $1/T$  in a log-linear scale. The solid line denotes the fit of the data to a VFT relation. The short dotted line denotes the fit to an Arrhenius law with the same prefactor  $1/D_0$ . (B) The average translational relaxation time  $\langle \tau_T \rangle$  obtained from QENS spectra in the same experimental conditions of the NMR experiment as a function of  $1/T$ . The dashed line denotes the VFT law fit, and the dotted line denotes the Arrhenius law fit with the same prefactor  $\tau_0$ . The values of fitting parameters are shown. Reprinted from ref. 55. Copyright (2006) National Academy of Sciences, U.S.A.

coefficient  $D$  and the average translational relaxation time  $\tau_T$  of water in the temperature range  $190$ – $280 \text{ K}$  using NMR and quasi-elastic neutron scattering (QENS) experiments, respectively. Note that it has not been possible to keep bulk water liquid below the homogeneous nucleation temperature ( $T_H$ ). (The  $T_H$  value of water at atmospheric pressure is something in between  $230$  and  $238 \text{ K}$ .<sup>71–75</sup>) Below  $T_H$ , water inevitably crystallizes to ice.<sup>76,77</sup> Therefore, the singular temperature  $T_S$  ( $228 \text{ K}$  at atmospheric pressure), at which the power-law divergence is seen in thermodynamic properties, is inaccessible. When the glassy form of water is heated above  $135 \text{ K}$  (the glass transition temperature  $T_G$  at atmospheric pressure) the glass-to-liquid phase transition occurs to form highly viscous liquid water, which crystallizes again at  $T_C \approx 150 \text{ K}$ .<sup>77–79</sup> Therefore, in between  $T_C$  and  $T_H$ , water does not exist in liquid form. This region is called the “no man’s land”.<sup>17</sup> Chen *et al.*<sup>55</sup> bypassed

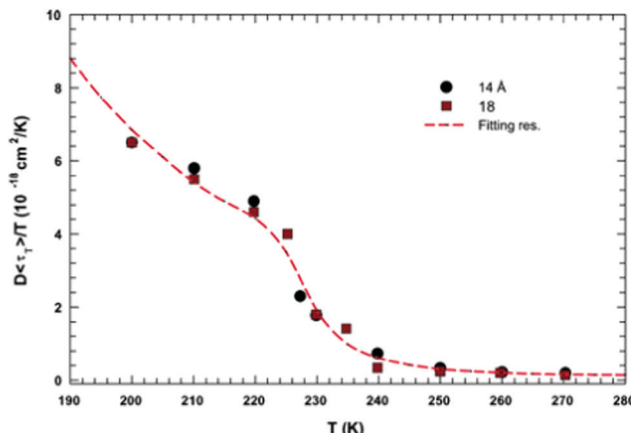


Fig. 2 The quantity  $D \langle \tau_T \rangle / T$  as a function of  $T$ . Dots and squares represent its values coming from the experimental data of  $D$  and  $\tau_T$  in samples with diameters of  $14$  and  $18 \text{ \AA}$ , respectively. The dotted line represents the same quantity obtained by using the fitting values obtained from the data reported in Fig. 1. Reprinted from ref. 55. Copyright (2006) National Academy of Sciences, U.S.A.

the above problem by supercooling water confined in one-dimensional hydrophilic silica pores, a suitable approach to study supercooled water below  $T_H$ .<sup>80–84</sup> The Arrhenius plots of  $D$  and  $\tau_T$  are presented in Fig. 1, where the transition from fragile (non-Arrhenius temperature dependence) to strong (Arrhenius temperature dependence) liquid is observed at  $\sim 225 \text{ K}$ . They also checked the validity of the SER for the entire range of temperature. An increasing breakdown of the SER was observed with decreasing temperature, as presented in Fig. 2. This breakdown is different on two sides of the fragile-to-strong dynamical transition point.

The MD simulation of the TIP5P model of water immediately supported the above experimental observation on the breakdown of the SER in supercooled water.<sup>58</sup> An increasing breakdown of the SER was observed in the simulation as the diffusion  $D$  decouples from the  $\alpha$ -relaxation time  $\tau_\alpha$ . There is a strong effect of pressure also.<sup>58</sup> Fig. 3a shows how the extent of the decoupling decreases with increasing pressure. This study proposed that the decoupling is somehow linked to the Widom line,<sup>85–89</sup> a hypothetical line emanates from the LLCP<sup>16</sup> and extends through  $T_W$ , the temperature at which the specific heat capacity is maximum. The simulated  $D\tau_\alpha/T$  lines for different pressures merge when the variable  $T$  is replaced by  $T-T_W$  at a given pressure.<sup>58</sup> The collapse is shown in Fig. 3b. A similar collapse was found for the temperature-dependent cluster size of the mobile molecules. Therefore, the breakdown of the SER in supercooled water was connected to the crossing of the Widom line associated with the liquid–liquid phase transition.

Some separate simulation studies of ST2 and SPC/E models of water provided an interesting insight into the breakdown of SER.<sup>57,59</sup> These studies considered two subsets of water molecules: one is highly mobile, and the other has the least mobility. The validities of SER and the Stokes–Einstein–Debye relation (SEDR) for these two separate subsets were checked. (The SEDR connects rotational diffusion with the viscosity of the medium.)

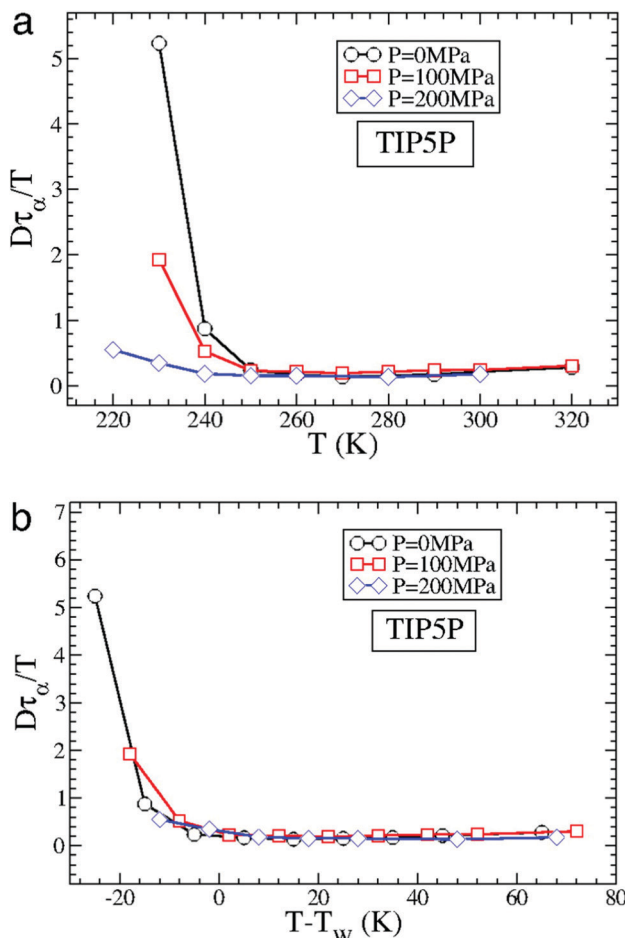


Fig. 3 How is the SER breakdown at low pressures correlated with the Widom line. (a)  $D\tau_z/T$  as a function of  $T$  for  $P = 0$  MPa, 100 MPa, and 200 MPa for the TIP5P model. Here,  $\tau_z$  is the  $\alpha$ -relaxation time. For all panels,  $D\tau_z/T$  is scaled by its high  $T$  value to facilitate the comparison of the different systems. (b)  $D\tau_z/T$  as a function of  $T - T_w(P)$  for TIP5P. The curves for different pressures overlap on the same master curve when  $T$  is replaced by  $T - T_w(P)$ . Adopted with permission from ref. 56. Copyright (2007) National Academy of Sciences, U.S.A.

Interestingly, both the relations did not hold at low temperatures for both the subsets. This contradicted the notion that the breakdowns of SER and SEDR originate only from the highly mobile molecules. An increasing decoupling between translational and rotational diffusion was found to be similarly strong in both subsets. To make a connection between the dynamical heterogeneities and breakdown of SER and SEDR, the time-dependence of the two relations was studied. Interestingly, both the translation-rotation decoupling and the breakdowns of SER and SEDR are strongest at a time scale corresponding to the end of the cage regime, when diffusion starts. Note that the dynamical heterogeneity is also maximum at the same time scale. This connects the breakdowns of the SER and SEDR with the dynamical heterogeneity of the medium.

Later, the mode-coupling theory-based calculation was performed.<sup>61</sup> Also, the study suggested that the violations of SER in the fragile liquid occur differently from that in the strong liquid region. It is worth mentioning that the fragile-to-strong

transition of liquid water, observed by Chen *et al.*<sup>55</sup> was also criticized in many articles.<sup>90</sup> Several works explained the above transition in terms of the finite-size effects, which decide the transition from liquid-like motion to localized motion near the glass transition temperature as observed in other nonaqueous glass-forming liquids.<sup>91–96</sup> It was argued that confinement can heavily influence the viscosity-controlled relaxation process at low temperatures. Several other groups questioned the analyses of Chen *et al.* and showed that the possibility of having the fragile-to-strong transition of water at the protein interface depends on the accuracy of the data analysis.<sup>97–100</sup> This debate continued attracting researchers to investigate the dynamical anomalies of supercooled water in greater detail.

A combined experiment and simulation study further investigated the microscopic origin of the breakdown of SER in supercooled water.<sup>60</sup> The diffusion coefficient starts following a fractional SER with structural relaxation time ( $D \sim \langle \tau_T \rangle / T^{-\zeta}$ ;  $\zeta \approx 3/5$ ) below 290 K. To understand the origin of this breakdown, FTIR spectra were analyzed to see the effect of temperature on the water OH-stretch over a temperature decreasing from 350 to 200 K. The results demonstrated that water forms low-density structure at lower temperature and therefore the breakdown of the SER in water may arise from the variation of the local water structure. An interesting explanation was given by Bagchi and coworkers using a two-state model of water: 5-coordinated high-density water and 4-coordinated low-density water.<sup>101,102</sup> They observed that the propagation of the 5-coordination defect occurs in a string-like path, the length of which increases with decreasing temperature. The propagation pathway resembles the Glarum defect.<sup>103</sup> The coordination number of the water molecules on the path is changed from 4 to 5 and then reverses back to 4 again. In this process, the tagged water molecule rotates by large angular jump following the Laage-Hynes jump mechanism.<sup>104,105</sup> The propagating defect gives rise to dynamical heterogeneity, which may be responsible for the breakdown of SER.

The LLCP and two-state model explanations of SER breakdown were seriously challenged by a study at high temperatures and pressures. The breakdown of both the SER and the SEDR were observed in a “hot liquid” state of water at 400 K and different pressures, ranging up to 3 GPa, the melting point of ice VII.<sup>106</sup> While the diffusion decreases and the viscosity increases with increasing pressure, the rate of reduction of diffusion decreases above 1 GPa pressure. This causes the breakdown of the SER. This result challenged the proposed theory, such as the LLCP hypothesis, two-state model, dynamic heterogeneity, *etc.*, for the breakdown of SER in supercooled water.

### 3.2 Direct verification of SER

Despite many studies provided important insights into the validity of the SER in supercooled water, these were somewhat indirect verifications. This is because of the usage of the average translational relaxation time  $\langle \tau_T \rangle$  or the  $\alpha$ -relaxation time  $\tau_z$  in place of the viscosity  $\eta$ . This is based on the assumption that the above relaxation times are linearly

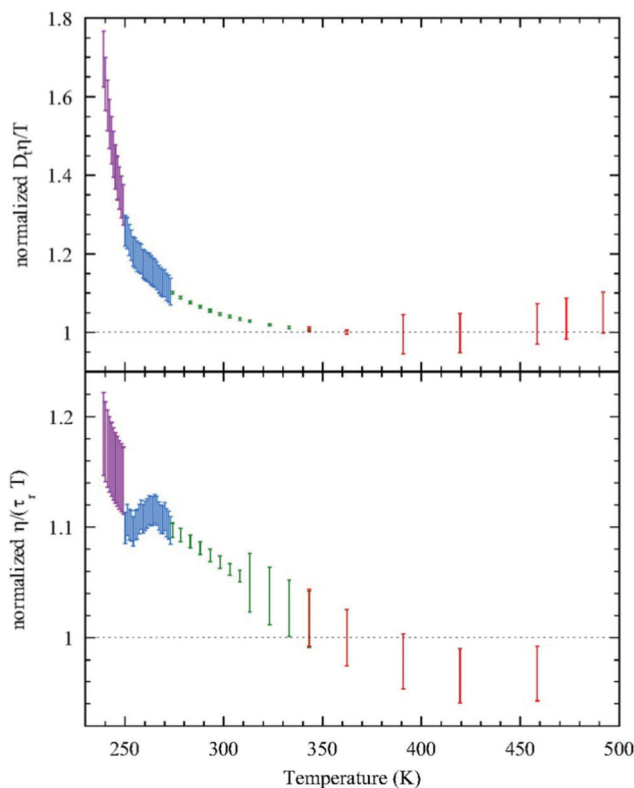


**Fig. 4** Test of the SER (upper panel) and SEDR (lower panel).  $D\eta/T$  (upper) and  $\eta/(\tau_r T)$  (lower) were plotted as a function of temperature. Here, the diffusion coefficient was denoted by  $D_r$ , while the molecular rotation time was denoted by  $\tau_r$ . The data were further normalized by their value at 362.25 K. The SER and SEDR relations would thus correspond to the horizontal dotted lines. SER and SEDR hold at high temperatures, but they are violated by around 70% and 18% at low temperatures, respectively. Reprinted with permission from ref. 54.

proportional to the viscosity  $\eta$ . Although  $\langle \tau_T \rangle$  is often coupled with  $\eta$ , there are many reports where this coupling does not strictly hold.<sup>107,108</sup> Therefore, it needs critical scrutiny and verification of the proportionality of  $\langle \tau_T \rangle$  with  $\eta$  before using  $\langle \tau_T \rangle$  in the SER.

Given this, it was suggestive to measure the viscosity of supercooled water and directly check the validity of SER. Dehaoui *et al.*<sup>54</sup> measured the viscosity of water most accurately at different temperatures down to 238 K. Using the literature diffusion coefficient<sup>109</sup> and single molecular rotation time<sup>110</sup> the authors checked the validities of SER and SEDR, respectively. As shown in Fig. 4, the SER increasingly breaks down with decreasing temperature while the SEDR remains valid in a wider range of temperatures. Unlike the usual glass formers, which show the breakdown of the SER only below  $1.3 T_g$ ,<sup>111–117</sup> for water the breakdown starts below  $2.1 T_g$ . In a follow-up experiment, Singh *et al.*<sup>48</sup> measured the viscosity at different  $T$ - $P$  thermodynamic state points. As the pressure increases at a constant temperature, the viscosity of water varies through a minimum value. The diffusion coefficient, on the other hand, varies through the maximum at a particular pressure. The locations of the above two extrema are sensitive to temperature. On reducing the temperature from 300 to 240 K, the location of

the viscosity minimum shifts towards higher pressure (from 80 MPa to 160 MPa) and the location of the diffusion maximum shifts from 100 MPa to 180 MPa pressure.<sup>48</sup> These are the dynamic anomalies, which were explained by the dynamic extension of the thermodynamic two-state model of water.<sup>41,45,118</sup> From the available diffusion and viscosity data at different  $T$ - $P$  state points the impact of pressure on the SER was also checked. The increasing pressure reduces the extent of breakdown of the SER at low temperatures.

Availability of the accurate viscosity coefficient data of supercooled water at different  $T$ - $P$  thermodynamic state points has triggered renewed interest in checking the validity of the SER in supercooled water. Several MD simulation-based investigations<sup>62–66,107,119,120</sup> have been carried out to provide more insights into the breakdown. The simulation study of the TIP4P/2005<sup>121</sup> model of water showed the breakdown.<sup>119</sup> In addition, the above study also focused on the breakdown or preservation of other non-standard forms of SER, like the coupling of diffusion with the H-bond lifetime,  $\alpha$ -relaxation time, *etc.* A separate MD simulation study<sup>107</sup> of TIP4P/2005f<sup>122</sup> water model reproduced the experimental diffusion and viscosity over a wide range of temperatures. The fact that the  $\alpha$ -relaxation time was decoupled from the viscosity at low temperatures suggested that the use of  $\alpha$ -relaxation time or average translational relaxation time might not be a foolproof way to check the validity of the SER. A more recent MD simulation study<sup>62</sup> of TIP4P/2005<sup>121</sup> water has addressed the impact of pressure on the SER breakdown in supercooled water. A dynamic extension of the thermodynamic two-state model of water<sup>41,45,118</sup> was used to explain the temperature- and pressure-dependent dynamical properties of water. In the two-state model, liquid water is considered as a mixture of two inter-converting species, a high-density state (HDS) and a low-density state (LDS). The violation of SER at lower temperatures was linked with the Widom line approach. Fig. 5 plots the normalized  $D\eta/T$  versus  $T-T_W(P)$ . Similar to that in Fig. 3b, an approximate collapse was observed when the normalized  $D\eta/T$

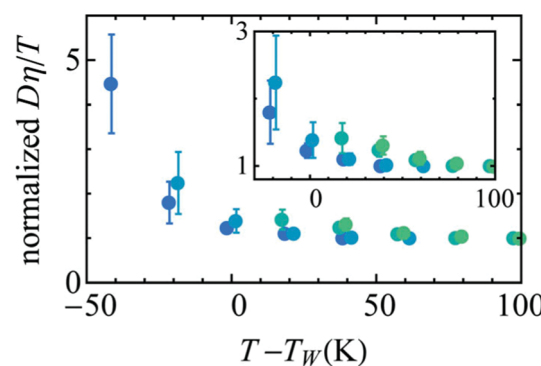


**Fig. 5** Temperature variation of the quantity  $D\eta/T$  normalized by its value at 300 K, as a function of the distance to the Widom line  $T-T_W(\rho)$  (see the text for details) for four isochrones (from bottom to top: 920.050, 960.090, 999.260, and 1040.59  $\text{kg m}^{-3}$ ). The inset points out the non-perfect collapse of the three isochrones. Reprinted from ref. 62, with the permission of AIP Publishing.

was plotted as a function of  $T-T_w(P)$ . However, the density dependence was still visible.

Although the above studies provided important insights into the breakdown of the SER, the molecular mechanism was still elusive. Although several scenarios, such as the Widom line approach, two-state model of water, the dynamic heterogeneity, *etc.*, were used to explain the breakdown of SER, a quantitative explanation was still necessary. Recently, our group has been able to explain the breakdown using the TJD approach.<sup>64–66</sup> The increasing importance of the translation jump-diffusion of water molecules with decreasing temperature was evidenced.<sup>64–66,123–125</sup> The presence of jump-diffusion in supercooled water was proposed earlier by many theoretical and simulation studies.<sup>124–132</sup> Goldstein's hypothesis<sup>133</sup> is worth mentioning. This hypothesis connected the temperature with the nature of translational diffusion of liquid molecules. According to this hypothesis, the translation of the liquid molecules occurs *via* jumping from one local free energy minima to another in the rugged free energy landscape at a lower temperature. However, with increasing temperature, the molecules gain thermal energy comparable to or higher than the free energy barrier heights and therefore diffuse freely *via* Brownian motion. Many theoretical and computer simulation studies<sup>126–132</sup> supported the above hypothesis and indicated the existence of translational jump in supercooled liquids. Previous studies have shown how the translational jump-diffusion of the solute from one solvent cage to another can be triggered by the translation-coupled-rotational pre-arrangement of nearby solvent water molecules around the solute.<sup>124,125</sup> The fragile-to-strong crossover has been seen to originate from the activated jump process, which dominates the dynamics in the deeply supercooled regime.<sup>134</sup>

Even though earlier studies hinted at the existence of the translational jump-diffusion and its role in various dynamic anomalies in supercooled water, including the breakdown of SER, more direct and quantitative evidence was still lacking. Our group estimated the jump-diffusion coefficient, which emanates from the jump-translation of water molecules, using a quantitative approach.<sup>64–66,123</sup> These studies quantified the contribution of jump-diffusion in the breakdown of SER in supercooled water at different  $T$ - $P$  thermodynamic state points. Apart from the neat supercooled water, the above method also explained the key aspects of SER breakdown in the binary mixture of water and methanol.<sup>66</sup> The contribution of the jump-diffusion was seen to be strongly connected with the structure of the liquid.<sup>64–66</sup> We detail the TJD approach and its usefulness for explaining the SER breakdown in the following section.

## 4. Breakdown of SER: explanation using the TJD approach

### 4.1 Calculation of diffusion $D$ and viscosity $\eta$ coefficients

Accurate determination of diffusion and viscosity coefficients is important to check the validity of SER. The diffusion coefficient

can be calculated using two routes. In the mean square displacement (MSD) route, the MSD is calculated for the molecules using the following equation,

$$\text{MSD} = \langle r^2(t) \rangle = \langle |r(t + t_0) - r(t_0)|^2 \rangle \quad (8)$$

Here,  $r(t_0)$  and  $r(t + t_0)$  are the positions of a molecule at times  $t_0$  and  $(t + t_0)$ , respectively. The brackets “ $\langle \rangle$ ” refer to the ensemble average. The simulated time-dependent MSD at long time are then fit to the linear equation, as per Einstein's diffusion equation,

$$\lim_{t \rightarrow \infty} r^2(t) = 6Dt \quad (9)$$

The diffusion  $D$  is calculated from the slope of the above equation.

The self-diffusion coefficient can also be calculated using the velocity autocorrelation function route,<sup>135</sup>

$$D = \frac{1}{3} \int_0^\infty \langle \mathbf{v}(t + t_0) \cdot \mathbf{v}(t_0) \rangle dt, \quad (10)$$

where  $\mathbf{v}(t + t_0)$  and  $\mathbf{v}(t_0)$  are the velocities of the particle at time  $t + t_0$  and time  $t_0$ , respectively. We used the MSD route for calculating the diffusion coefficient.<sup>64–66,123,125</sup>

The viscosity coefficient can be calculated using the Green–Kubo formula<sup>63,136–138</sup>

$$\eta = \frac{V}{10k_B T} \int_0^\infty \sum_{\alpha\beta}^9 \langle P_{\alpha\beta}(0) P_{\alpha\beta}(t) \rangle dt \quad (11)$$

Here,  $k_B$  is the Boltzmann constant,  $V$  is the volume of the box, and  $T$  is the temperature of the system. The brackets “ $\langle \rangle$ ” refer to the ensemble average.  $P_{\alpha\beta}$ , the symmetrized traceless portion of the stress tensor  $\sigma_{\alpha\beta}$ , can be defined as

$$P_{\alpha\beta} = \frac{1}{2} (\sigma_{\alpha\beta} + \sigma_{\beta\alpha}) - \frac{1}{3} \delta_{\alpha\beta} \left( \sum_{\alpha} \sigma_{\alpha\alpha} \right) \quad (12)$$

$\delta_{\alpha\beta}$  is the Kronecker delta and there are six, out of the nine, distinct  $P_{\alpha\beta}$  elements. Note that eqn (11) improves the statistics over the original Green–Kubo relation, which considers the average of only three off-diagonal terms.

$$\eta = \frac{V}{3k_B T} \int_0^\infty \left\langle \sum_{\alpha\beta}^3 P_{\alpha\beta}(0) P_{\alpha\beta}(t) \right\rangle dt \quad (13)$$

However, eqn (11) and (13) do not result in significantly different  $\eta$  values when sufficiently long simulation trajectories are examined.<sup>64–66</sup>

### 4.2 The steps of the TJD approach in chronology

Here, we detail the method of estimating the jump-diffusion coefficient  $D_{\text{Jump}}$ . Accurate identification of a translational jump is one of the most crucial steps. The simplest method is *via* monitoring the displacement of a molecule from its initial position over time and identifying a jump event by a sudden change of displacement.<sup>124,125,139–142</sup> Being a visual identification-based method it cannot quantitatively estimate  $D_{\text{Jump}}$ . In addition, this approach fails to identify all jumps and thus undermines the contribution of  $D_{\text{Jump}}$  in total

diffusion.<sup>124</sup> Some more quantitative methods are present in the literature.<sup>130</sup> The jump-diffusion of a model glass-forming liquid was estimated using a method that assumed that the timescale of fluctuation of a caged particle's position is of the order of the Debye–Waller (DW) factor.<sup>130</sup> A translational jump is thus defined by a fluctuation of larger magnitude compared to the DW factor. The oscillator model theory-based approach was used to calculate the jump-diffusion of a small tracer in a glass-forming liquid.<sup>143,144</sup> These methods were used in usual glass-forming liquids but not in supercooled water.

Our method of calculating  $D_{\text{Jump}}$  is based on a technique introduced by Raptis *et al.*<sup>145,146</sup> and modified by Araque *et al.*<sup>147</sup> The steps are listed in chronological order.

(I) The first step involves the calculation of the non-Gaussian parameter  $\alpha_2(t)$ <sup>135,148</sup> using the following equation,

$$\alpha_2(t) = 3r^4(t)/5r^2(t)^2 - 1, \quad (14)$$

where  $r^2(t) = |\mathbf{r}(t + t_0) - \mathbf{r}(t_0)|^2$  and  $r^4(t) = |\mathbf{r}(t + t_0) - \mathbf{r}(t_0)|^4$ . Here,  $\mathbf{r}(t_0)$  and  $\mathbf{r}(t + t_0)$  are the positions of a molecule at time  $t_0$  and  $(t + t_0)$ , respectively. The brackets “ $\langle \rangle$ ” refer to the ensemble average.  $\alpha_2(t)$  goes through a maximum value at the characteristic time  $t = t^*$ .

(II) The long trajectory of a water molecule is split into smaller trajectory segments, each of duration  $t^*$ . The consideration of  $t^*$  comes from the fact that the transition from the sub-diffusive cage regime to the diffusive regime of the mean square displacement (MSD) occurs at time  $t^*$ . Also, at this time the dynamical heterogeneity is seen to be maximum. However, the results do not change appreciably with a slight deviation of time from  $t^*$ .<sup>64</sup> Let us assume that the splitting of a full molecular trajectory, of duration  $t_{\text{traj}}$ , into equal segments of  $t^*$  length, produces  $M$  smaller trajectory segments. Therefore,  $M = t_{\text{traj}}/t^*$ . Also, in each trajectory segment, we have  $n$  number of time steps.

(III) The radii of gyration are calculated for all the  $M$  smaller trajectory segments. The radius of gyration for  $i$ th smaller trajectory segment  $R_{g,i}$  ( $1 \leq i \leq M$ ) is calculated using the following equation,<sup>64–66,145–147</sup>

$$R_{g,i} = \sqrt{\frac{1}{n} \sum_{(i-1)t^* \leq t \leq it^*} |\mathbf{r}(t) - \mathbf{r}_{\text{CM},i}|^2} \quad (15)$$

Here,  $\mathbf{r}(t)$  is the molecule's position at time  $t$  and  $\mathbf{r}_{\text{CM},i}$  is the center-of-mass of the  $i$ th trajectory segment, which is calculated using the following equation,<sup>64–66,145–147</sup>

$$\mathbf{r}_{\text{CM},i} = \frac{1}{n} \sum_{(i-1)t^* \leq t \leq it^*} \mathbf{r}(t) \quad (16)$$

(IV) The net displacements in the  $i$ th trajectory segment  $\lambda_i$  is twice that of  $R_{g,i}$

$$\lambda_i = 2R_{g,i} \quad (17)$$

(V) It is obvious that every smaller trajectory segments are not jump-trajectories. Therefore, one needs to categorically identify the jump-trajectory segments. This can be done based on a distance criterion, which is obtained by following the

deviation of the self-part of the van Hove correlation function at a time  $t^*$ ,  $G_s(r, t^*)$ , from the Gaussianity.<sup>64–66,147</sup>  $G_s(r, t^*)$  provides the probability distribution of displacement at time  $t^*$  and is calculated using the following equation,<sup>64–66,135,148</sup>

$$G_s^{\text{simu}}(r, t^*) = \delta(r - |\mathbf{r}(t_0) - \mathbf{r}(t_0 + t^*)|) \quad (18)$$

Here,  $\mathbf{r}(t_0)$  and  $\mathbf{r}(t_0 + t^*)$  are the positions of a molecule at a time  $t_0$  and  $(t_0 + t^*)$ , respectively. To see the deviation of the simulated self-part of the van Hove correlation function from the Gaussianity, we compare  $G_s^{\text{simu}}(r, t^*)$  with the following Gaussian equation,

$$(G_s^{\text{theo}}(r, t^*)) = \left[ \frac{3}{2\pi r^2(t^*)} \right]^{\frac{3}{2}} \exp \left[ -\frac{3r^2}{2r^2(t^*)} \right], \quad (19)$$

where  $r^2(t^*)$  is the MSD at the time  $t^*$ ,  $r^2(t^*) = |\mathbf{r}(t_0 + t^*) - \mathbf{r}(t_0)|^2$ . In presence of the translational jump occurrences,  $G_s^{\text{simu}}(r, t^*)$  has a pronounced tail beyond the distance  $r_2$ , where  $G_s^{\text{simu}}(r, t^*)$  crosses  $G_s^{\text{theo}}(r, t^*)$ . In this regime, molecules displace more than expected from the Gaussian distribution. Thus we consider a molecular trajectory segment as a jump one if the molecule translates more than  $r_2$  in that segment. Therefore, the  $i$ th trajectory segment is a jump-trajectory if it follows the condition,  $\lambda_i > r_2$ .  $G_s^{\text{simu}}(r, t^*)$  also crosses  $G_s^{\text{theo}}(r, t^*)$  at a lower  $r$ -value,  $r = r_1$ , below which the molecules move less than expected from the Gaussian distribution. These trajectories are called cage-trajectories. While the identification of the jump-trajectory segments is the key for calculating the jump-diffusion coefficient, the identification of cage-trajectory segments serves nothing in the TJD approach but visual confirmation of correct classification of different trajectory types using the above protocol (see Fig. 9).

(VI) As the jump-trajectory segments are identified, we count the number of such jump-trajectories for all the molecules present in the system. We assume that a total number of jump trajectory segments for all the molecules is  $N_{\text{Jump}}$ . The jump-diffusion coefficient  $D_{\text{Jump}}$  can be calculated using the jump frequency  $\nu_{\text{Jump}}$  and average square jump length  $\lambda_{\text{Jump}}^2$ <sup>64–66,123</sup> via the following equation,

$$D_{\text{Jump}} = \frac{1}{6} \nu_{\text{Jump}} \lambda_{\text{Jump}}^2, \quad (20)$$

Eqn (20) can be derived from the random walk problem.<sup>64</sup> We have presented the derivation of the equation in the Appendix. Here, the jump frequency,  $\nu_{\text{Jump}}$  and average square jump length  $\lambda_{\text{Jump}}^2$  can be written as,

$$\nu_{\text{Jump}} = \frac{N_{\text{Jump}}}{Nt_{\text{traj}}} \text{ and } \lambda_{\text{Jump}}^2 = \lim_{N_{\text{Jump}} \rightarrow \infty} \frac{1}{N_{\text{Jump}}} \sum_{j=1}^{N_{\text{Jump}}} \lambda_j^2, \quad (21)$$

where  $N_{\text{Jump}}$  is the total number of jump events for all the molecules  $N$  and  $t_{\text{traj}}$  is the full simulation trajectory length.  $\lambda_j^2$  is the square jump length for the  $j$ th jump-trajectory segment ( $1 \leq j \leq N_{\text{Jump}}$ ) of some molecule in the system.

(VII) Note that  $D_{\text{Jump}}$  originates from only the jump-trajectory segments. The remaining trajectory segments provide another component of the total diffusion  $D$ . We denote the

other component as the residual-diffusion  $D_{\text{Res}}$ , which emanates from the small-step displacement of the molecules. Therefore, the total diffusion coefficient  $D$  can be written as the sum of  $D_{\text{Jump}}$  and  $D_{\text{Res}}$ . Thus,  $D_{\text{Res}}$  can be calculated by subtracting  $D_{\text{Jump}}$  from  $D$ .<sup>64–66,123</sup>

$$D_{\text{Res}} = D - D_{\text{Jump}} \quad (22)$$

Since  $D_{\text{Res}}$  emanates from the small-step displacement of the molecules  $D_{\text{Res}}$  must follow the SER. One of the key steps of the TJD approach is to check whether  $D_{\text{Res}}$  follows SER. We will see in the next sections that indeed  $D_{\text{Res}}$  follows the SER. This proves the role of  $D_{\text{Jump}}$  in the breakdown of SER.

#### 4.2. Applications of the TJD approach

In this section, we discuss some instances, where the TJD approach successfully explained the breakdown of the SER.

**4.2.1 Pure supercooled water.** The experiments were performed in pure supercooled water to check the validity of the SER at different temperatures and pressures.<sup>48,54</sup> Our first goal was to obtain the simulated diffusion and viscosity coefficient values at different thermodynamic states in good agreement with the experimental data. Water molecules were simulated at various temperatures between 210 K and 300 K at 1 bar pressure. Fig. 6a and b present the Arrhenius plots for simulated  $D$  (system-size-corrected<sup>64,65,149–151</sup>) and  $\eta$  values, which are in excellent agreement with the experimental values,<sup>54,109</sup> presented in the same figures. As summarized in Section 4.1, we calculated the diffusion coefficient using the MSD route and viscosity using the Green-Kubo relation.<sup>64–66</sup> The simulated  $D$  and  $\eta$  values are a good fit to the empirical

Vogel–Fulcher–Tamman (VFT) equation.<sup>62,64,107,119</sup> We also fit the simulated  $D$  and  $\eta$  using the power-law equation,<sup>54,152–154</sup> which provides equally good fit over the full temperature range. This is consistent with the experiment.<sup>54</sup> The caption of Fig. 6 presents the fitting equations and their parameters for both simulated  $D$  and  $\eta$ . These simulated  $D$  and  $\eta$  values at different temperatures were used to check the validity of the SER. As per eqn (7), the normalized  $D\eta/T$  (the normalization was done at 300 K) value must be unity irrespective of the temperature. However, that is not the case here. Fig. 6c shows that the normalized  $D\eta/T$  starts increasing from unity as the temperature is decreased below 300 K and reaches  $\sim 3.5$  at 210 K. This suggests an increasing breakdown of the SER with decreasing temperature. Consistent with the experimental results, the fitting of the simulated  $D$  and  $\eta$  values with the equation  $D \propto (\eta/T)^\xi$  provides  $\xi = -0.85$ .<sup>54,155</sup>

In separate work,<sup>65</sup> the simulated  $D$  and  $\eta$  values of water were reported at different  $T$ – $P$  thermodynamic state points. The simulated values are consistent with the experiment.<sup>48</sup> Ten different temperatures between 220 and 340 K and six different pressures between 0 and 250 MPa were considered. Fig. 7a and b present the pressure-dependent  $D$  and  $\eta$  values. Consistent with the experimental result,<sup>48,151,159</sup> the pressure-dependent dynamical anomalies are more evident at lower temperatures ( $T < 270$  K). The normalized  $D\eta/T$  values are presented in Fig. 7c. Above 300 K, the  $D\eta/T$  value remains almost constant at unity for all pressures. However,  $D\eta/T$  increases from unity with decreasing temperature, which suggests the breakdown of the SER. The extent of breakdown decreases with increasing pressure.

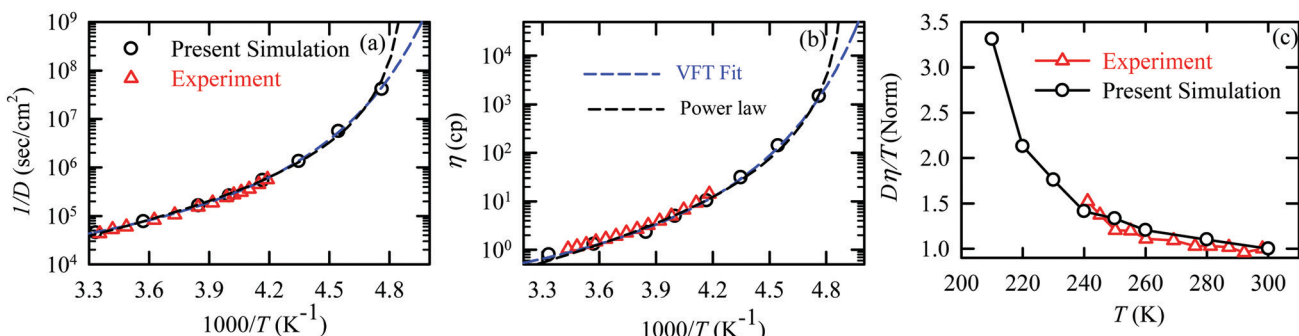


Fig. 6 The Simulated<sup>64,65,149–151</sup> and experimental<sup>54,109</sup> transport properties as function of temperature. The Arrhenius plot of diffusion coefficient  $D$  (a) and viscosity coefficient  $\eta$  (b). (c) The temperature-dependent normalized  $D\eta/T$  values where the normalization is done at  $T = 300$  K. The red triangles represent the experimental values, while the simulated values are represented by black circles in all three panels. The simulated diffusion and viscosity values are fitted with the power-law (black dashed line) and VFT equation (blue dashed line) in both (a and b). The fitting parameters of the power-law equation for the diffusion coefficient  $D = D_0 \left[ \frac{T - T_s}{T_s} \right]^{-\gamma}$  are:  $\gamma = -2.60$ ,  $D_0 = 1.71 \times 10^{-4}$  cm<sup>2</sup> s<sup>-1</sup>, and  $T_s = 204.28$  K ( $\chi^2 = 23.64$ ) and for the viscosity coefficient are:  $\eta = \eta_0 \left[ \frac{T - T_s}{T_s} \right]^{-\gamma}$  are:  $\gamma = 2.97$ ,  $\eta_0 = 0.065$  cp and  $T_s = 203.24$  K ( $\chi^2 = 1.95$ ). The simulated singular temperature  $T_s$  for both the diffusion and viscosity coefficients are approximately 15 K less than  $T_s$  obtained by fitting the experimental data.<sup>54</sup> The fitting parameters of the VFT equation for the diffusion coefficient  $D = D_0 e^{\left[ \frac{-B}{T - T_0} \right]}$  are:  $D_0 = 3.05 \times 10^{-4}$  cm<sup>2</sup> s<sup>-1</sup>,  $B = 328.34$  K, and  $T_0 = 175.54$  K ( $\chi^2 = 2.576$ ) and for the viscosity coefficient  $\eta = \eta_0 e^{\left[ \frac{-B}{T - T_0} \right]}$  the fitting parameters are:  $\eta_0 = 3.85 \times 10^{-2}$  cp,  $B = -360.34$  K, and  $T_0 = 175.60$  K ( $\chi^2 = 0.469$ ). The fittings are done using the non-linear chi-square fitting method<sup>156</sup> with the weights calculated from the standard errors.<sup>64</sup> We have also used the Marquardt–Levenberg algorithm,<sup>157,158</sup> which is a least square method, to find the fitting parameters, which are presented in Fig. S1 of the ESI.† Adopted with permission from ref. 64. Copyright (2019) American Chemical Society.

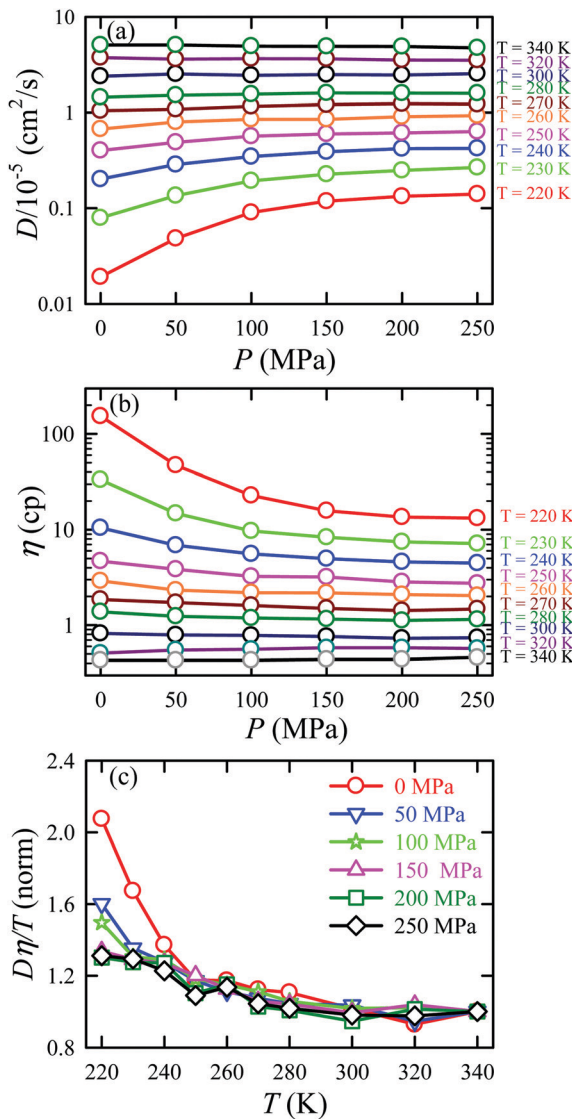


Fig. 7 Pressure dependence diffusion coefficients (a) and viscosity coefficient  $\eta$  (b), and normalized  $D\eta/T$  values (c) at all temperatures. The normalization of  $D\eta/T$  values is performed at  $T = 340$  K. Reprinted with permission from ref. 65. Copyright (2019) American Chemical Society.

We applied the TJD approach to explaining the breakdown of SER. First,  $D_{\text{Jump}}$  was calculated following the steps, detailed in Section 4.2. Next, the residual-diffusion coefficient  $D_{\text{Res}}$  was calculated by subtracting  $D_{\text{Jump}}$  from  $D$  (eqn (22)). Finally, we checked whether the normalized  $D_{\text{Res}}\eta/T$  remained unity irrespective of temperature and pressure.<sup>64</sup> This would confirm the role of jump-diffusion for the breakdown of the SER in super-cooled water. The non-Gaussian parameters  $\alpha_2(t)$ , calculated using eqn (14) for the temperatures between 210 K and 300 K, are presented in Fig. 8a. On decreasing temperature from 300 K to 210 K, the characteristic time  $t^*$  increases from  $\sim 1$  ps to  $\sim 560$  ps.<sup>64</sup> Also, the increase of pressure decreases  $t^*$ .<sup>65</sup> Following step (I), the simulation trajectories were divided into smaller segments, each of duration  $t^*$ . As per step (II),  $R_{g,i}$  were

calculated for each smaller trajectory segments (eqn (15)). Next,  $\lambda_i$  was calculated for all water molecules in the  $i$ th trajectory segment using eqn (17). The distance criteria for jump-trajectory segment were obtained by comparing the simulated  $G_S^{\text{simu}}(r,t^*)$  (eqn (18)) with the theoretical  $G_S^{\text{theo}}(r,t^*)$  (eqn (19)). A sample comparison is shown in Fig. 8b for  $T = 210$  K and 1 bar pressure. As discussed in step (V), the criteria for a jump-trajectory segment is  $\lambda_i > r_2$ . Fig. 8c presents a sample of  $\lambda_i$  for a particular water molecule during 100 ns simulation trajectory at 210 K. The jump-trajectories are those for which  $\lambda_i$  crosses  $r_2$  cutoff line. Fig. 9 presents some examples of the jump and cage-trajectory segments at 210 and 250 K temperatures. Clearly the protocol for identification of the jump-trajectory segments seemed working properly.

The jump-diffusion coefficient  $D_{\text{Jump}}$  was calculated (eqn (20)) using the jump frequency  $\nu_{\text{Jump}}$  and average square jump length  $\lambda_{\text{Jump}}^2$  (eqn (21)). Fig. 10a presents  $\chi_{\text{Jump}} = 100 \times (D_{\text{Jump}}/D)$  as a function of temperature.<sup>64–66,123</sup>  $\chi_{\text{Jump}}$  depicts the percentage contribution of the jump-diffusion in total diffusion. Starting from a negligible value at 300 K,  $\chi_{\text{Jump}}$  increases with decreasing temperature and reaches almost 50% at 210 K.<sup>64</sup> The SER for  $D_{\text{Jump}}$  is shown in Fig. 10b. As expected,  $D_{\text{Jump}}$  is strongly decoupled from the viscosity. Finally, eqn (22) was used to calculate the residual-diffusion coefficient  $D_{\text{Res}}$  by subtracting  $D_{\text{Jump}}$  from  $D$ . Fig. 10c plots the normalized  $D_{\text{Res}}\eta/T$  as a function of temperature. The normalization was done at 300 K. The comparison between  $D\eta/T$  and  $D_{\text{Res}}\eta/T$  plots, one of the most important results, shows that while  $D\eta/T$  increases with decreasing temperature,  $D_{\text{Res}}\eta/T$  remains almost constant with decreasing temperature.<sup>64</sup> This strongly suggests that the jump-diffusion is responsible for the breakdown of the SER since the exclusion of the jump-diffusion leads to the diffusion-viscosity coupling at any temperature.

$D_{\text{Jump}}$  was also calculated at different  $T$ - $P$  thermodynamic state points in a separate work.<sup>65</sup> Fig. 11a shows how  $\chi_{\text{Jump}}$  varies with temperature for different pressures.  $\chi_{\text{Jump}}$  decreases with increasing pressure at a given temperature. So, the jump-diffusion is more prevalent at lower temperatures and pressures. Fig. 11b plots the normalized  $D_{\text{Jump}}\eta/T$  values as a function of temperature for all pressures. Evidently,  $D_{\text{Jump}}$  is strongly decoupled from viscosity at any  $T$ - $P$  state points, suggesting  $D_{\text{Jump}}$  as a natural violator of the SER. Fig. 11c presents the normalized  $D_{\text{Res}}\eta/T$  as a function of temperature for all the pressures. Fascinatingly, the normalized  $D_{\text{Res}}\eta/T$  for all pressures merged with one other approximately at unity. Therefore  $D_{\text{Res}}$  couples with the viscosity of the medium sufficiently strongly and follow the SER for all  $T$ - $P$  thermodynamic state points. Therefore, these studies provided the most conclusive evidence of the role of translational jump-diffusion of water molecules for the breakdown of the SER.

**4.2.2 Aqueous binary mixture.** The TJD approach was also used for explaining the breakdown of the SER in a binary mixture of water and methanol.<sup>66</sup> The diffusion coefficient of water in water/methanol binary mixture was measured by the NMR-based pulsed gradient stimulated spin-echo technique (<sup>1</sup>H-PGSTE).<sup>160</sup> It is worth mentioning that the proton exchange

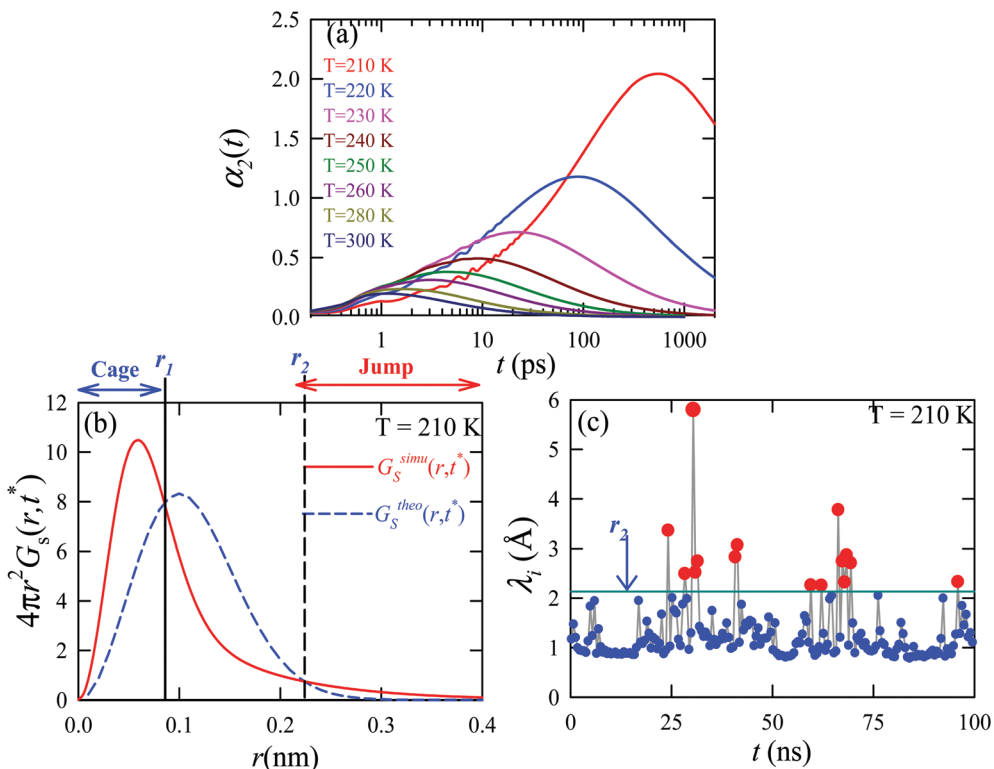


**Fig. 8** (a) The non-Gaussian parameters for all the temperatures studied. (b) The comparison between the simulated self-part of the van Hove correlation function  $G_s^{\text{simu}}(r, t^*)$  (solid line) and the corresponding theoretical one ( $G_s^{\text{theo}}(r, t^*)$ ) (dashed line) at time  $t^*$ . (c) The distance traversed by one water molecule,  $\lambda_i$ , in the  $i^{\text{th}}$  trajectory segment at 210 K. The peak intensity beyond  $r_2$  distance presents the jump-trajectory segments. Reprinted with permission from ref. 64. Copyright (2019) American Chemical Society.

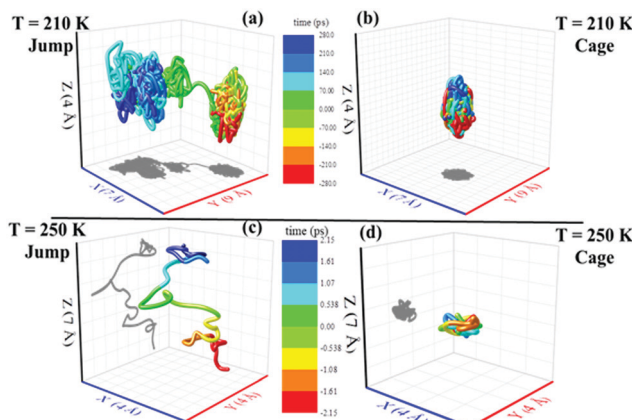


**Fig. 9** Representative jump and cage-trajectories at  $T = 210$  and  $250$  K. Panels (a) and (c) represent jump-trajectory segments, while panels (b) and (d) represent cage-trajectory segments. The color mapping represents the time evolution of a trajectory. Reprinted with permission from ref. 64. Copyright (2019) American Chemical Society.

event from water to the OH group of the methanol molecule may somewhat affect the diffusion coefficient of water. However, this is not clear how this proton exchange biases the measured diffusion coefficient of water. Using the experimentally measured  $D$  and  $\eta$  for pure water,<sup>54,109,161,162</sup> pure methanol,<sup>163–169</sup> and water/methanol binary mixtures<sup>160,170–173</sup>

of different mixture compositions at different temperatures the role of binary mixture composition on the validity of the SER was investigated.<sup>160</sup> The simulated overall diffusion  $D$ , diffusion of water  $D_W$ , diffusion of methanol  $D_M$ , and  $\eta$  values<sup>66</sup> are plotted against temperature for different binary mixture compositions in Fig. 12. We compare the simulated  $D_W$  of water in the mixture and the simulated  $D_M$  of methanol in pure methanol with the available experimental diffusion coefficients in Fig. 12b and c, respectively. These show reasonably good agreement between the simulated and experimental diffusion values. Some differences between simulation and experimental data are observed at lower temperature especially for the equimolar mixture. Both the simulated  $D$  and  $\eta$  values changed non-monotonically with the methanol mole-fraction  $x_M$  above 250 K. However, the non-monotonicity decreases with decreasing temperature.

The validity of SER was checked by plotting the normalized  $D\eta/T$  values in Fig. 13 for the overall system, water, and methanol. In all cases, the normalized  $D\eta/T$  gradually increase from unity as the temperature was decreased, which suggests increasing violation of the SER. While intense breakdowns of the SER were observed in pure supercooled water, the SER remained almost valid for pure methanol. Methanol concentration had a strong effect on the breakdown of the SER in the water/methanol binary mixture. Above 260 K, the most intense violation of the SER was observed for the equimolar mixture,

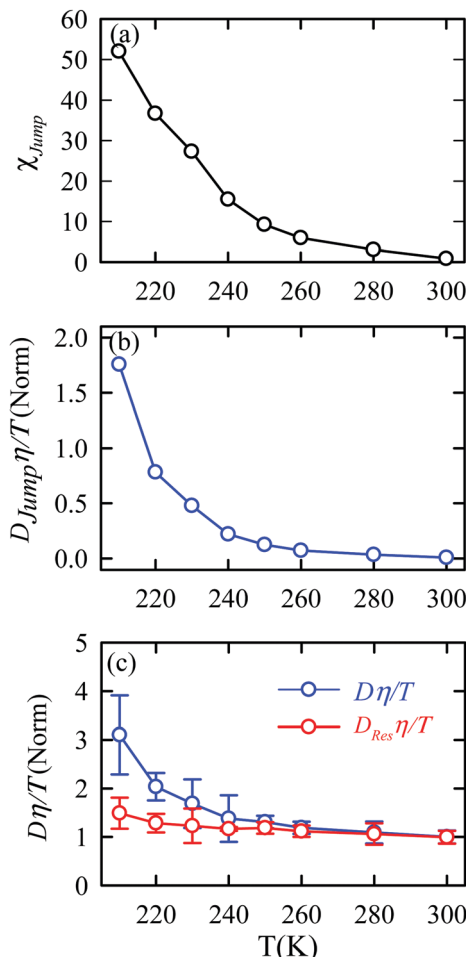


Fig. 10 (a) Temperature dependence of the percentage contribution of jump-diffusion in total diffusion,  $\chi_{\text{Jump}}$ . (b) Coupling of  $D_{\text{Jump}}$  with the medium viscosity  $\eta$  at different temperatures. (c) Coupling of total diffusion  $D$  and the residual-diffusion coefficient  $D_{\text{Res}}$  with medium viscosity  $\eta$  at different temperatures. The error bars in panel (c) are the standard deviations. Adopted with permission from ref. 64. Copyright (2019) American Chemical Society.

which is consistent with the experiment.<sup>160</sup> However, at the lowest temperature 220 K, the extent of the breakdown of SER decreases with increasing methanol concentration.

The effect of methanol concentration on the breakdown of the SER in the water/methanol binary mixture was explained using the TJD approach.  $D_{\text{Jump}}$  was calculated for each system using the steps detailed in Section 4.2. Different parameters in the jump-diffusion analysis, like  $t^*$ ,  $\alpha_2(t^*)$ ,  $\nu_{\text{Jump}}$  etc. showed non-monotonic composition dependence with the maximum at  $x_M \sim 0.5$ .<sup>66</sup> The above non-monotonicity was gradually reduced with decreasing temperature.  $\chi_{\text{Jump}}$ , for the overall system, is plotted as a function of  $x_M$  at different temperatures in Fig. 14a.  $\chi_{\text{Jump}}$  increases with decreasing temperature for all the binary mixture compositions. The composition dependence on  $\chi_{\text{Jump}}$  was also interesting. At 300 K, for pure water and pure methanol,  $\chi_{\text{Jump}}$  was negligible, while for the equimolar mixture  $\chi_{\text{Jump}}$  was  $\sim 8\%$ . This astounding increase of

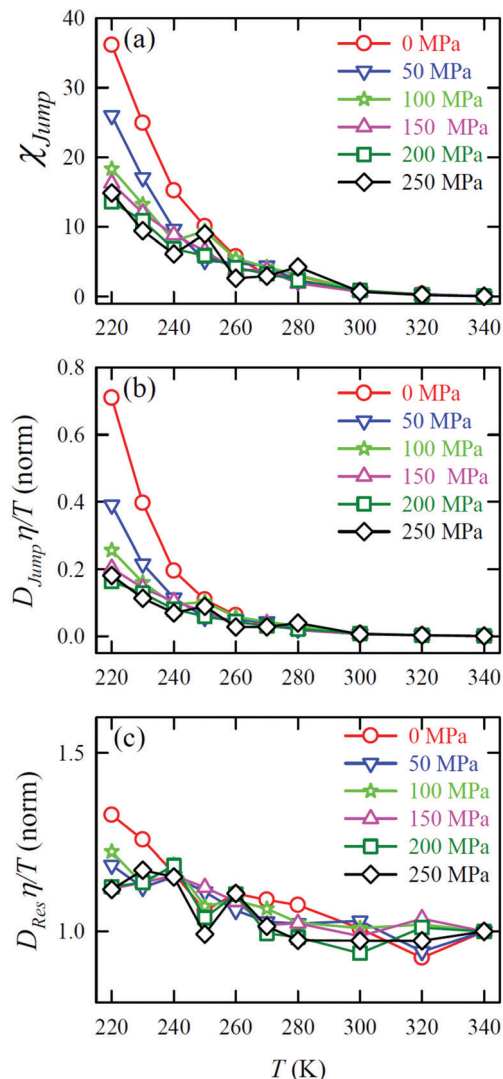
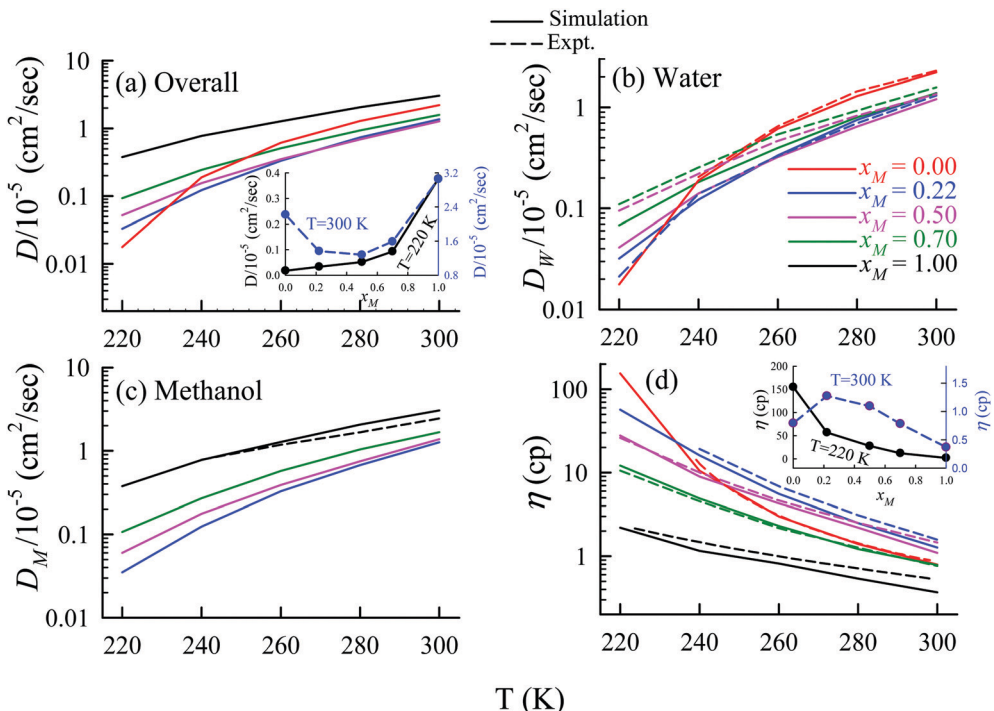


Fig. 11 (a) Temperature-dependent percentage contribution  $\chi_{\text{Jump}}$  for different pressures. (b) Normalized  $D_{\text{Jump}}\eta/T$ , and (c) Normalized  $D_{\text{Res}}\eta/T$  as functions of temperature for all pressures. The normalization is done at  $T = 340$  K. Reprinted with permission from ref. 65. Copyright (2019) American Chemical Society.

$\chi_{\text{Jump}}$  for  $x_M = 0.5$  suggested a larger extent of the SER breakdown in the equimolar mixture observed in the experiment. The increase of  $\chi_{\text{Jump}}$  with decreasing temperature is maximum for pure water. Approximately 40 times increase of  $\chi_{\text{Jump}}$  was reported for pure water, while the increase is only 6 times for  $x_M = 0.5$  due to the decrease of temperature from 300 K to 220 K. Finally,  $D_{\text{Res}}$  for the overall system, water, and methanol were calculated and the normalized  $D_{\text{Res}}\eta/T$  values were plotted *versus*  $T$  for different compositions. These are presented in Fig. 14b-d. Interestingly,  $D_{\text{Res}}$  remains fairly coupled to the viscosity of the medium almost at all temperatures and mixture compositions. This is true for the overall system, water, and methanol. However, the values are somewhat scattered (0.7–1.2) at temperatures below 240 K, particularly for the overall system.



**Fig. 12** Comparison between simulated (solid line) and experimental (dashed line) transport coefficients. (a) Temperature-dependent overall self-diffusion coefficient  $D$  for different systems. The inset shows the non-monotonic composition dependence of  $D$  at 300 K and monotonic composition dependence at 220 K. (b and c) Temperature-dependent diffusion coefficients of water ( $D_W$ ) and methanol ( $D_M$ ), respectively. (d) Temperature-dependent shear viscosity coefficient ( $\eta$ ) for different systems. The inset of (d) shows the non-monotonic composition dependence of  $\eta$  at 300 K and monotonic composition dependence at 220 K. Reprinted with permission from ref. 66. Copyright (2020) American Chemical Society.

### 4.3. Connection between Jump-diffusion and liquid structure

The previous sections have detailed how the TJD approach successfully explained the breakdown of SER in pure super-cooled water, and water/methanol binary mixture from the jump-diffusion perspective. The effect of pressure, temperature, and mixture composition on  $\chi_{\text{Jump}}$  was already revealed. But what is the more fundamental origin of the jump-diffusion? In this section, we put forward some possible connections between the jump-diffusion and water structure. The local structure of water, analyzed by the average number of H-bonds per water molecule  $n_{\text{Hb}}$  and the tetrahedral order parameter  $q$ , was examined at different  $T$ - $P$  thermodynamic state points. The H-bond between two water molecules was characterized by the following distance and angle criteria:<sup>104,174–177</sup>  $r_{\text{ODOA}} < 3.5 \text{ \AA}$ ,  $r_{\text{OAHD}} < 2.45 \text{ \AA}$ , and  $\angle \text{H}_D \text{O}_D \text{O}_A < 30^\circ$ , where the H-bond donor and acceptor are defined by “D” and “A”, respectively. The tetrahedral order parameter  $q$  of a tetrahedral structure was calculated using the following equation,<sup>178–183</sup>

$$q = 1 - \frac{3}{8} \sum_{j=1}^3 \sum_{k=j+1}^4 \left( \cos \theta_{jk} + \frac{1}{3} \right)^2, \quad (23)$$

where  $\theta_{jk}$  is the angle between the vectors joining two nearby water molecules with the central water molecule.  $\langle q \rangle = 0$  stands for an entirely random configuration, like an ideal gas, while  $\langle q \rangle = 1$  represents a perfectly tetrahedral geometry.

Fig. 15a presents the temperature-dependent  $n_{\text{Hb}}$  of water at different pressures. Evidently, below 290 K,  $n_{\text{Hb}}$  decreases with increasing pressure, while  $n_{\text{Hb}}$  increases with decreasing pressure above 290 K temperature. Fig. 15b shows that  $\chi_{\text{Jump}}$  behaves systematically with  $n_{\text{Hb}}$ .  $\chi_{\text{Jump}}$  is increased with  $n_{\text{Hb}}$  almost exponentially irrespective of temperature and pressure. Since  $n_{\text{Hb}}$  is the strength of trapping a water molecule, the more is the value of  $n_{\text{Hb}}$  the larger the trapping force. Therefore, the increase of  $\chi_{\text{Jump}}$  with the increase of  $n_{\text{Hb}}$  gives a clear sign that the diffusion of a trapped water molecule is more dominated by jump-diffusion. Therefore, the stronger trapping of a molecule triggers more translational-jump-dominated diffusion. The average tetrahedral order parameter  $\langle q \rangle$  of water is presented in Fig. 16a for different  $T$ - $P$  thermodynamic state points. Also, Fig. 16b shows a very strong correlation between  $\langle q \rangle$  and  $\chi_{\text{Jump}}$ . As the order of the water molecules increases and water–water H-bond strength increases, the water molecules increasingly diffuse *via* the jump-diffusion mechanism.

Apart from the H-bonding and the tetrahedral ordering of water, there is another factor that also dictates whether the jump-diffusion is the key diffusion channel in a binary mixture of water and methanol. This is the structural inhomogeneity of the system, particularly for a binary mixture. At 300 K,  $\chi_{\text{Jump}}$  is maximum ( $\sim 8\%$ ) for the equimolar mixture. This large increase of  $\chi_{\text{Jump}}$  at  $x_M = 0.5$  is primarily responsible for the maximum SER breakdown for the equimolar mixture.

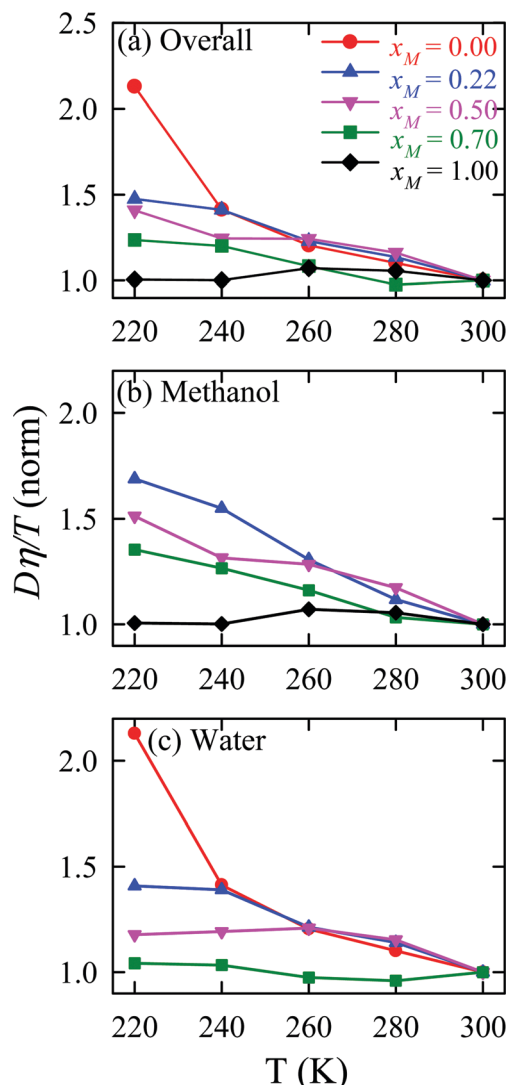


Fig. 13 Temperature-dependent normalized  $D\eta/T$  values for (a) the overall system, (b) methanol, and (c) water for different compositions. The normalization is done at 300 K. Reprinted with permission from ref. 66. Copyright (2020) American Chemical Society.

as seen in the experiment. However, this non-monotonic behavior is reduced by decreasing the temperature. It was found that the above increase of  $\chi_{\text{Jump}}$  in the equimolar methanol/water binary mixture is connected to the dynamic heterogeneity, which was measured by the area under the  $G_s(r, t^*)$  curve  $\phi$  beyond the distance  $r_2$ ,<sup>184–187</sup> the distance criteria for jump-diffusion. The enclosed area  $\phi$  is shown in Fig. 17. Fig. 18 presents  $\phi$  as a function of the methanol concentration at different temperatures. The non-monotonic composition dependence of  $\chi_{\text{Jump}}$  is evident at 300 K. However, the non-monotonicity is reduced by the decrease of temperature. The equimolar water/methanol mixture is dynamically more heterogeneous. Methanol induces microheterogeneity in the aqueous solution even at room temperature, which is akin to other similar aqueous binary mixtures.<sup>188–201</sup>

## 5. Conclusion and future scope

In this article, we have reviewed significant works focusing on the breakdown of the SER in supercooled water. Although prior studies have provided some theoretical explanations for the observed breakdown of the SER, we have not yet reached a consensus. Because of the presence of the homogeneous nucleation temperature of the water, it is practically impossible to keep bulk water liquid below  $T_H$ . To avoid the crystallization of water, earlier experiments considered confined water for studying the SER validity. We have reviewed the studies, which measured the average translational relaxation time instead of viscosity of the medium for checking the validity of SER in indirect means. However, with the progress of advanced experimental techniques, it has been recently possible to measure the viscosity of bulk supercooled water at different  $T$ - $P$  thermodynamic state points accurately. The breakdown of SER was observed directly using the measured diffusion and viscosity for the wide range of temperature and pressure. The key findings of these studies are reviewed here.

We have also reviewed the theoretical and MD simulation studies, which significantly contributed to understanding the breakdown of SER. The LLCP-based approach showed the onset of the breakdown of the SER as the crossing of the Widom line. The  $D\eta/T$  lines for different pressures collapse into one line when the variable  $T$  is replaced by  $T-T_W$  at a given pressure; where  $T_W$  is the Widom line temperature. The increasing breakdown of SER with decreasing temperature of the supercooled water was linked to the increasing dynamical heterogeneity of the medium. A dynamical version of the thermodynamic two-state model of water was also used to explain the temperature- and pressure-dependent diffusion and viscosity of water. The two-state model considered liquid water to be a mixture of HDS and LDS. The breakdown of the SER at lower temperatures was explained in connection with the Widom line defined by an equal fraction of these two states. However, the above approaches were seriously challenged by a study reporting the breakdown of the SER of water at very high pressure (in the order of GPa) and the temperature at which water cannot be thought of as a mixture of two states.

An alternate explanation for the breakdown of SER was given by our group. This is the TJD approach, which has been reviewed here in detail. First, the steps for estimating the jump-diffusion coefficient are listed. Further, we have detailed few examples, where the TJD approach successfully explained the breakdown of SER in pure supercooled water and water/methanol binary mixture. The translational jump-diffusion coefficient was calculated for supercooled water at different  $T$ - $P$  thermodynamic state points and a binary mixture of water and methanol at different temperatures and compositions. The jump-diffusion coefficient was then subtracted from the total diffusion coefficient to obtain the residual-diffusion coefficient. The validity of the SER for the residual-diffusion coefficient, instead of the total diffusion coefficient, proves the role of jump-diffusion in the breakdown of the SER. Finally, we made an effort to connect the jump-diffusion with the microscopic

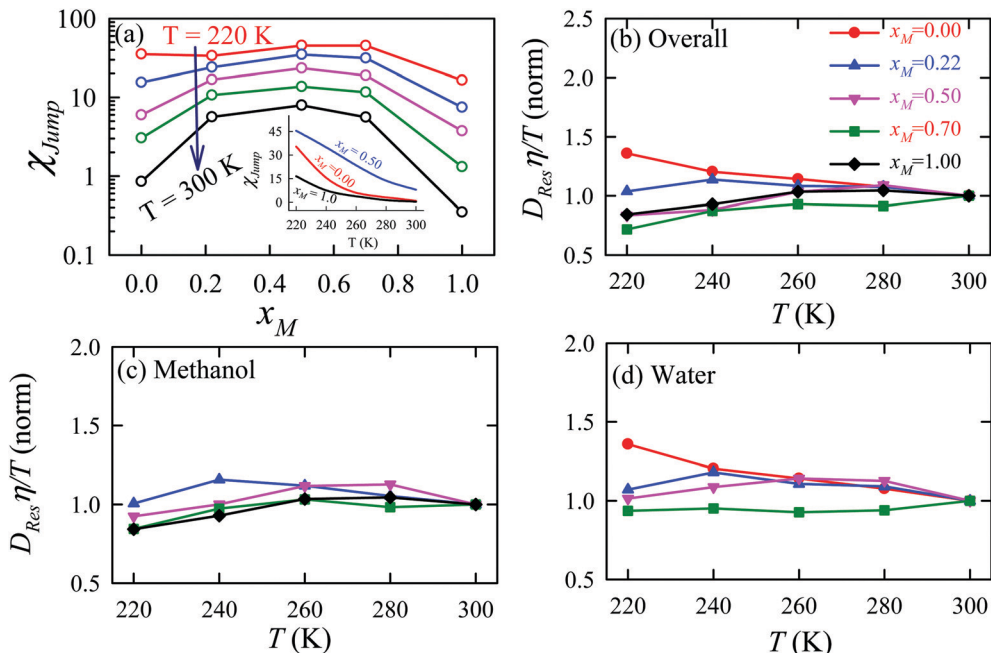


**Fig. 14** (a) Methanol concentration dependences of  $\chi_{Jump}$ , the percentage contribution of jump-diffusion  $D_{Jump}$  in the total diffusion  $D$ , at different temperatures: 220 K (red), 240 K (blue), 260 K (pink), 280 K (dark green), and 300 K (black). The inset in panel (a) presents the temperature dependence of  $\chi_{Jump}$  at three different mole fractions: pure water, pure methanol, and equimolar water/methanol binary mixture. Temperature-dependent normalized  $D_{Res}\eta/T$  for the (b) overall system, (c) methanol, and (d) water. The normalizations were done at 300 K. Adopted with permission from ref. 66. Copyright (2020) American Chemical Society.

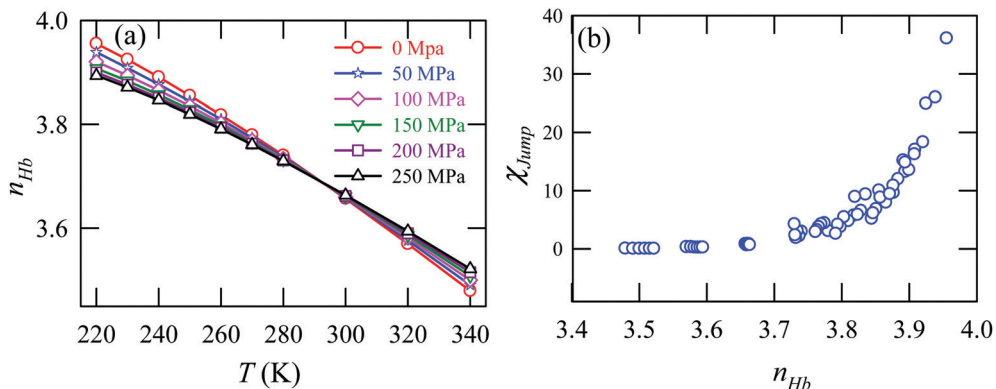


**Fig. 15** (a) The average number of hydrogen bonds per water molecule  $n_{Hb}$  at different temperatures and pressures. (b)  $\chi_{Jump}$  as a function  $n_{Hb}$ . Reprinted with permission from ref. 65. Copyright (2019) American Chemical Society.

structure of water. As the tagged water molecule is more strongly arrested by neighboring water molecules it diffuses more *via* jump translation. This correlation is important in explaining the breakdown of the SER.

We now comment on the timescale relevant to the breakdown of the SER in the general supercooled liquid. Kaufman and coworkers<sup>202</sup> calculated frequency-dependent diffusion and viscosity coefficients to check the validity of the generalized SER. The authors found that the SER is valid to a good approximation at the frequencies that are associated with the  $\beta$ -relaxation regime when the particles rattle inside the cage. The authors argued that although the  $\beta$ -relaxation regime is

dynamically heterogeneous the SER remains valid and therefore they concluded that the dynamical heterogeneity does not necessitate the breakdown of the SER. This was opposite to the general notion that the breakdown of the SER stems from the heterogeneous dynamics of the system having both highly mobile and least mobile particles.<sup>117</sup> Note that the above conclusion was drawn based on the non-Gaussian parameter  $\alpha_2(t)$ . However, there is an intense debate on the actual time scale depicting the dynamical heterogeneity and the SER breakdown. Instead of using  $\alpha_2(t)$ , Szamel and coworkers<sup>203</sup> proposed a new non-Gaussian parameter  $\gamma(t)$  that weights the immobile particles which move less than expected from the Gaussian

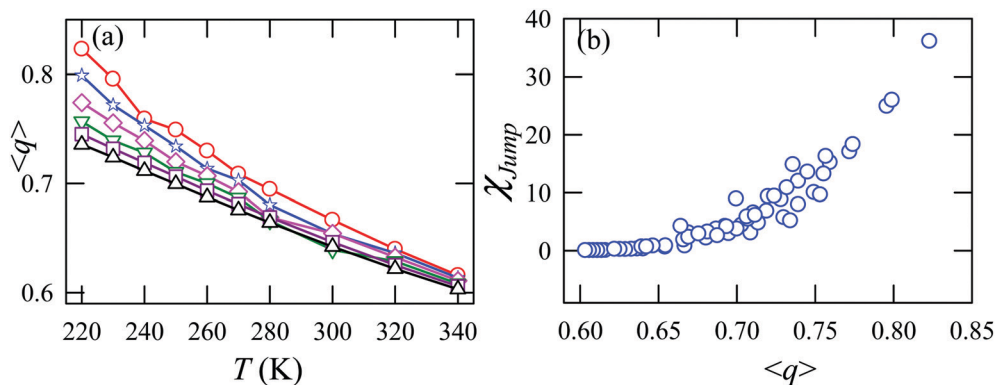


Fig. 16 (a) The average tetrahedral order parameter ( $\langle q \rangle$ ) at different temperatures and pressures. (b)  $\chi_{\text{Jump}}$  as a function of  $\langle q \rangle$ . Reprinted with permission from ref. 65. Copyright (2019) American Chemical Society.

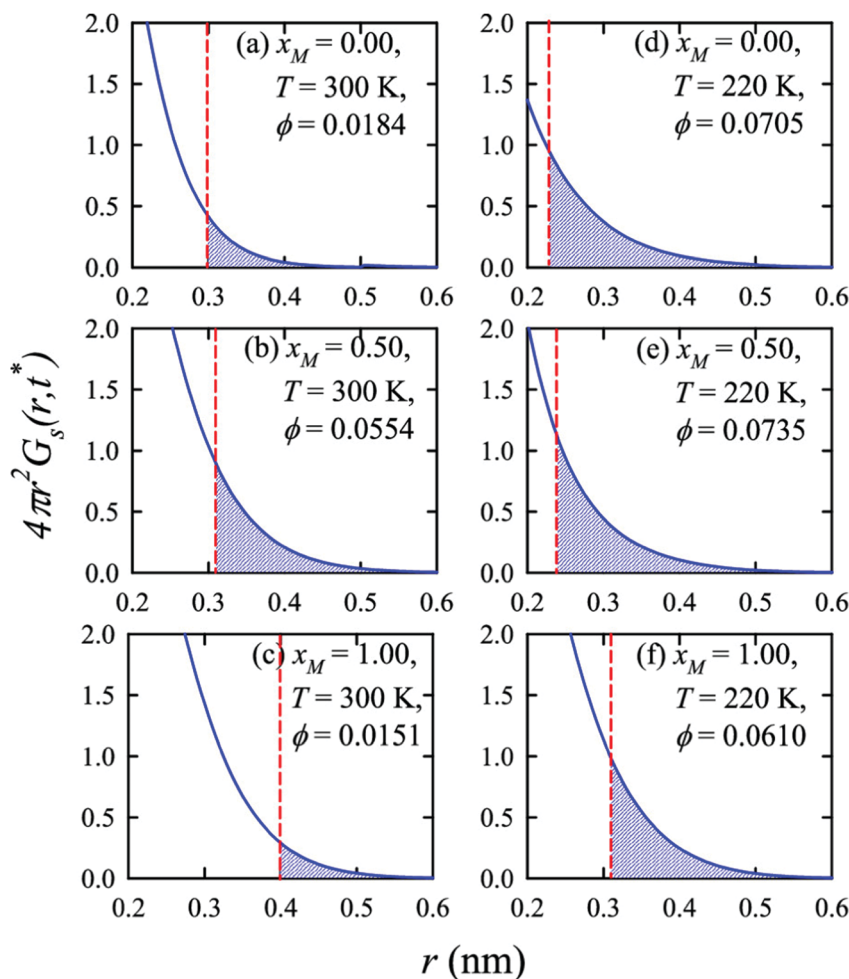


Fig. 17 Exponential decays of the simulated self part of the van Hove correlation function at time  $t^*$ , when  $\alpha_2(t)$  is maximum, for three different compositions ( $x_M = 0.0, 0.5, 1.0$ ) and two temperatures (220 K and 300 K). The shaded part is the area  $\phi$  under a curve beyond  $r_2$  distance. The vertical dashed lines indicate the  $r_2$  distance. Reprinted with permission from ref. 66. Copyright (2020) American Chemical Society.

distribution. It was found that  $\gamma(t)$  performs better than  $\alpha_2(t)$  as far as the heterogeneity timescale is concerned. Although at a higher temperature, the peak positions for  $\alpha_2(t)$  and  $\gamma(t)$  are

same, the peak position of  $\alpha_2(t)$  increases slower than  $\gamma(t)$  with decreasing temperature. Studies by Kim and Saito investigated the lifetime of dynamical heterogeneity in supercooled

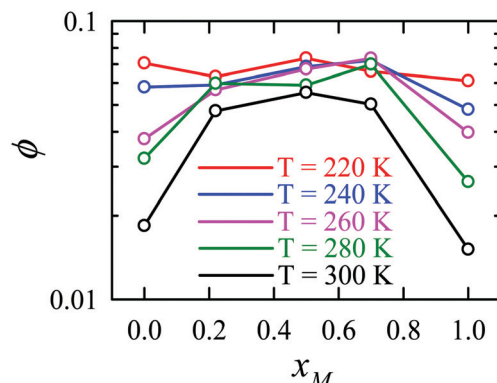


Fig. 18 The area under the curve, shown in Fig. 17, as a function of mixture composition at different temperatures. Reprinted with permission from ref. 66. Copyright (2020) American Chemical Society.

liquids using a four-point, three-time density correlation function.<sup>204,205</sup> They examined the physical role of the lifetime of dynamical heterogeneity  $\tau_{\text{hetero}}$  in the breakdown of SER by calculating the frequency-dependent viscosity and self-diffusion constant.<sup>206</sup> At low temperatures, a strong breakdown of SER was observed at lower frequencies. The characteristic time scale of the violation is in accord with  $\tau_{\text{hetero}}$ . Therefore the dynamical heterogeneity is directly linked to the violation of the SE relation in supercooled liquids. These studies raised an important point about the actual timescale concerning the dynamic heterogeneity and breakdown of the SER in supercooled water. In the heterogeneous dynamics, the jump diffusion of particles are responsible for the breakdown of the SER. One can address how these different timescales contribute to the breakdown of SER *via* the present TJD approach.

Finally, we comment here on the future scope of the TJD approach. Even though the above approach has been used only in pure bulk water and a binary mixture of water and methanol, this approach has potential application in various problems. The following are some of the problems one can study using the TJD approach. (i) Although we have considered here only the supercooled water, very similar behaviors are seen for other liquids also. Diffusion in mediums, such as room temperature ionic liquids (RTILs)<sup>147,207–212</sup> deep eutectic systems (DES),<sup>213–217</sup> phase change material (PCM),<sup>218–221</sup> usual glass-forming liquids,<sup>222–230</sup> and polymeric material,<sup>231–236</sup> show a strong breakdown of the SER. The TJD approach may provide insights into this problem. For understanding in a crowded environment or highly heterogeneous medium, position-dependent diffusion and friction might be relevant.<sup>237–242</sup> (ii) The experimental observation on the breakdown of the SER in water at extreme pressure (GPa range) and temperature challenged the usual concept of hot dense water behaving as a simple liquid.<sup>106</sup> The LLCP hypothesis and the two-state model of water seem to fail in explaining the breakdown of the SER in the above  $T$ – $P$  region. The present TJD approach can provide new insights into the breakdown of the SER in this regime. (iii) Hopping dynamics of molecules in a biological system are

important. The hopping of lipid molecules from one domain to another in the biological cell membrane is important in various contexts, such as protein trafficking, cell signaling, *etc.*<sup>243–252</sup> The TJD approach, with necessary modification, can be used for understanding the hopping dynamics of the lipid molecules and elucidating allied biological problems. This approach can be also used to understand the diffusive dynamics of protein and water in its hydration shells<sup>188,217,253–257</sup> (iv) The quantum effect on dynamics of water is very important, particularly in the deeply supercooled regime near the glass transition temperature.<sup>258</sup> A number of studies have suggested that the quantum fluctuation partially disrupts the H-bonding network of water.<sup>258,259</sup> The less structured H-bonding network, compared to that in the classical counterpart, somewhat reduces the viscosity of the medium and enhances the translational and rotational diffusion of the molecules.<sup>258,260–268</sup> Although the quantum effects of different dynamical properties of supercooled water are studied the quantum effect on the validity of the SER remains largely unaddressed. This might be an important topic to address in the future using the TJD approach.

## Abbreviations

1H-PGSTE	1H-Pulsed gradient stimulated spin-echo technique
CPF	Critical-point-free
DW	Debye–Waller
FTIR	Fourier transform infrared spectroscopy
HDL	High-density liquid
HDS	High-density state
LDL	Low-density liquid
LDS	Low-density state
LLCP	Liquid–liquid critical point
MD	Molecular dynamics
MSD	Mean square displacement
QENS	Quasi-elastic neutron scattering
SER	Stokes–Einstein relation
SEDR	Stokes–Einstein–Debye relation
SFA	Singularity free approach
SLC	Stability-limit conjecture
TIP4P/2005	Transferrable intermolecular potential four point/2005
TIP5P	Transferrable intermolecular potential five point
TJD	Translational Jump-diffusion
TMD	Temperature of maximum density
VFT	Vogel–Fulcher–Tamman

## Conflicts of interest

There are no conflicts to declare.

## Appendix

We assume that the translational jumps of molecules are not correlated and statistically independent from each other. Therefore, the current problem effectively turns into the random walk problem.<sup>10</sup> For simplicity, we derive for 1D random

walk. As per the definition of the random walk, the probability of moving along the positive  $x$ -axis is equal to the probability of moving along the negative  $x$ -axis. Let us assume the total number of jumps of a molecule is  $n_{\text{Jump}}$ . Let us suppose that a jumping molecule takes displacement  $s_j$  because of the  $j$ th jump occurrence. Note that unlike  $\lambda_i$ , which is always positive,  $s_j$  can be either positive or negative. Due to the number of jumps, the effective displacement of a molecule is:

$$x = \sum_{j=1}^{n_{\text{Jump}}} s_j. \quad (\text{A1})$$

These jumps are assumed to be completely independent of each other. The average over many replicas of the random walk is

$$x = \sum_{j=1}^{n_{\text{Jump}}} s_j = 0. \quad (\text{A2})$$

Similarly, we can calculate the average square displacement as

$$x^2 = \sum_{i=1}^{n_{\text{Jump}}} \sum_{j=1}^{n_{\text{Jump}}} s_i s_j = \sum_{i=1}^{n_{\text{Jump}}} \sum_{j=1}^{n_{\text{Jump}}} s_j^2 \delta_{ij}. \quad (\text{A3})$$

Therefore, we can write

$$x^2 = \sum_{j=1}^{n_{\text{Jump}}} s_j^2. \quad (\text{A4})$$

Therefore, the variance can be written as,

$$\Delta x^2 = x^2 - x^2 = \sum_{i=1}^{n_{\text{Jump}}} s_j^2. \quad (\text{A5})$$

Now, for three dimensions, we can write,

$$\Delta r^2 = \sum_{j=1}^{n_{\text{Jump}}} \lambda_j^2 = n_{\text{Jump}} \lambda_{\text{Jump}}^2, \quad (\text{A6})$$

where  $\lambda_j^2$  is square jump distance in three-dimension for the  $j$ th jump-trajectory segment.  $\lambda_{\text{Jump}}^2$  is the average square jump distance, which can be written as,

$$\lambda_{\text{Jump}}^2 = \lim_{n_{\text{Jump}} \rightarrow \infty} \frac{1}{n_{\text{Jump}}} \sum_{j=1}^{n_{\text{Jump}}} \lambda_j^2 \quad (\text{A7})$$

$r^2$  at the final time of the trajectory,  $t_{\text{traj}}$  can be obtained also from Einstein's equation

$$r^2 = 6D_{\text{Jump}} t_{\text{traj}}. \quad (\text{A8})$$

Comparing eqn (A6) and (A8), we obtain the expression of  $D_{\text{Jump}}$  as

$$D_{\text{Jump}} = \frac{1}{6} \nu_{\text{Jump}} \lambda_{\text{Jump}}^2 \quad (\text{A9})$$

where  $\nu_{\text{Jump}}$ , the jump frequency, can be written as,

$$\nu_{\text{Jump}} = n_{\text{Jump}}/t_{\text{traj}} \quad (\text{A10})$$

and  $\lambda_{\text{Jump}}^2$  is calculated using eqn (A7).

Although the eqn (A9) is derived for one particle, we can analyze the trajectories of all  $N$  molecules, present in the system and calculate the jump-diffusion coefficient using eqn (A9). However, the calculations of  $\nu_{\text{Jump}}$  and  $\lambda_{\text{Jump}}^2$  consider all jump occurrences in the system. If the total number of jump occurrences is  $N_{\text{Jump}}$  for all the  $N$  molecules, we can write the expression of  $\nu_{\text{Jump}}$  and  $\lambda_{\text{Jump}}^2$  as following,

$$\nu_{\text{Jump}} = \frac{N_{\text{Jump}}}{N t_{\text{traj}}} \text{ and } \lambda_{\text{Jump}}^2 = \lim_{N_{\text{Jump}} \rightarrow \infty} \frac{1}{N_{\text{Jump}}} \sum_{j=1}^{N_{\text{Jump}}} \lambda_j^2 \quad (\text{A11})$$

$$D_{\text{Jump}} = \frac{1}{6} \left( \frac{N_{\text{Jump}}}{N t_{\text{traj}}} \right) \lambda_{\text{Jump}}^2 = \frac{1}{6} \nu_{\text{Jump}} \lambda_{\text{Jump}}^2.$$

Here  $\nu_{\text{Jump}}$  is the jump frequency (number of jump occurrences per molecule in unit time) and  $\lambda_{\text{Jump}}^2$  is the average square jump length, averaged over all the jump events in the system  $N_{\text{Jump}}$ . So, we can write the expressions of  $\nu_{\text{Jump}}$  and  $\lambda_{\text{Jump}}^2$  as follows:

$$\nu_{\text{Jump}} = \frac{N_{\text{Jump}}}{N t_{\text{traj}}}, \quad (\text{A12})$$

and

$$\lambda_{\text{Jump}}^2 = \lim_{N_{\text{Jump}} \rightarrow \infty} \frac{1}{N_{\text{Jump}}} \sum_{i=1}^{N_{\text{Jump}}} \lambda_i^2 \quad (\text{A13})$$

## Acknowledgements

We acknowledge IIT Patna and the SERB Early Career Research Award (ECR/2017/002335) for funding. We acknowledge the anonymous reviewers for their great suggestions to improve the quality of the MS. We acknowledge Dr Premashis Manna and Mr Tonmoy Sharma for assisting in curve fitting. We acknowledge Dr Sandipa Indra for her contribution in the initial works on solute's translational jump diffusion in super-cooled water. We are grateful to Prof. Pratim K. Chattaraj for his strong support. We thank Prof. James T. Hynes and Prof. Ranjit Biswas for their encouragement. We appreciate Ms Shakkira Erimaban, and Ms Archita Maiti for their valuable inputs. We dedicate this article in memory of S.D.'s beloved grandmother Late Kanak Lata Daschakraborty.

## References

1. P. Gallo, K. Amann-Winkel, C. A. Angell, M. A. Anisimov, F. d. r. Caupin, C. Chakravarty, E. Lascaris, T. Loerting, A. Z. Panagiotopoulos and J. Russo, *Chem. Rev.*, 2016, **116**, 7463–7500.
2. F. Franks, *Water: a matrix of life*, Royal Society of Chemistry, 2000.
3. F. Franks, *Water A Comprehensive Treatise: Volume 4: Aqueous Solutions of Amphiphiles and Macromolecules*, Springer US, 2013.
4. P. G. Debenedetti, *Metastable liquids: concepts and principles*, Princeton University Press, 1996.

5 P. G. Debenedetti, *J. Phys.: Condens. Matter*, 2003, **15**, R1669.

6 P. G. Debenedetti and H. E. Stanley, *Phys. Today*, 2003, **56**, 40–46.

7 C. A. Angell, *Annu. Rev. Phys. Chem.*, 2004, **55**, 559–583.

8 P. Ball, *Chem. Rev.*, 2008, **108**, 74–108.

9 M.-C. Bellissent-Funel, *Hydration processes in biology: Theoretical and experimental approaches*, IOS Press, 1999.

10 M. W. Evans, G. W. Robinson, S. Singh and S.-B. Zhu, *Water in biology, chemistry and physics: experimental overviews and computational methodologies*, World Scientific, 1996.

11 C. A. Angell, *Annu. Rev. Phys. Chem.*, 1983, **34**, 593–630.

12 D. S. Eisenberg and W. Kauzmann, *The structure and properties of water*, Oxford University Press, Oxford, 2005.

13 L. G. M. Pettersson, R. H. Henchman and A. Nilsson, *Chem. Rev.*, 2016, **116**, 7459–7462.

14 S. Saito and B. Bagchi, *J. Chem. Phys.*, 2019, **150**, 054502.

15 S. Saito, I. Ohmine and B. Bagchi, *J. Chem. Phys.*, 2013, **138**, 094503.

16 P. H. Poole, F. Sciortino, U. Essmann and H. E. Stanley, *Nature*, 1992, **360**, 324–328.

17 O. Mishima and H. E. Stanley, *Nature*, 1998, **396**, 329–335.

18 H. E. Stanley and V. K. Wong, *Am. J. Phys.*, 1972, **40**, 927–928.

19 P. Kumar and H. E. Stanley, *J. Phys. Chem. B*, 2011, **115**, 14269–14273.

20 C. Angell, W. Sichina and M. Oguni, *J. Phys. Chem.*, 1982, **86**, 998–1002.

21 H. Sato, K. Watanabe, J. Levelt Sengers, J. S. Gallagher, P. G. Hill, J. Straub and W. Wagner, *J. Phys. Chem. Ref. Data*, 1991, **20**, 1023–1044.

22 O. Conde, J. Teixeira and P. Papon, *J. Chem. Phys.*, 1982, **76**, 3747–3753.

23 H. Kanno and C. Angell, *J. Chem. Phys.*, 1979, **70**, 4008–4016.

24 C. Bertrand and M. Anisimov, *J. Phys. Chem. B*, 2011, **115**, 14099–14111.

25 C. Jeffery and P. Austin, *J. Chem. Phys.*, 1999, **110**, 484–496.

26 S. Kiselev, *Int. J. Thermophys.*, 2001, **22**, 1421–1433.

27 S. Kiselev and J. Ely, *J. Chem. Phys.*, 2002, **116**, 5657–5665.

28 J. Kalova and R. Mares, *Int. J. Thermophys.*, 2010, **31**, 756–765.

29 P. H. Poole, F. Sciortino, U. Essmann and H. E. Stanley, *Phys. Rev. E: Stat. Phys., Plasmas, Fluids, Relat. Interdiscip. Top.*, 1993, **48**, 3799.

30 P. H. Poole, U. Essmann, F. Sciortino and H. E. Stanley, *Phys. Rev. E: Stat., Nonlinear, Soft Matter Phys.*, 1993, **48**, 4605.

31 F. Sciortino, P. H. Poole, U. Essmann and H. Stanley, *Phys. Rev. E: Stat. Phys., Plasmas, Fluids, Relat. Interdiscip. Top.*, 1997, **55**, 727.

32 S. Sastry, P. G. Debenedetti, F. Sciortino and H. E. Stanley, *Phys. Rev. E: Stat. Phys., Plasmas, Fluids, Relat. Interdiscip. Top.*, 1996, **53**, 6144.

33 C. A. Angell, *Science*, 2008, **319**, 582–587.

34 P. Chitnelawong, F. Sciortino and P. H. Poole, *J. Chem. Phys.*, 2019, **150**, 234502.

35 R. J. Speedy, *J. Phys. Chem.*, 1982, **86**, 982–991.

36 E. Lascaris, *Phys. Rev. Lett.*, 2016, **116**, 125701.

37 D. Fuentevilla and M. Anisimov, *Phys. Rev. Lett.*, 2006, **97**, 195702.

38 V. Holten and M. Anisimov, *Sci. Rep.*, 2012, **2**, 1–7.

39 H. Stanley, P. Kumar, G. Franzese, L. Xu, Z. Yan, M. G. Mazza, S. Buldyrev, S.-H. Chen and F. Mallamace, *Eur. Phys. J.: Spec. Top.*, 2008, **161**, 1–17.

40 L. Xu, P. Kumar, S. V. Buldyrev, S.-H. Chen, P. H. Poole, F. Sciortino and H. E. Stanley, *Proc. Natl. Acad. Sci. U. S. A.*, 2005, **102**, 16558–16562.

41 H. Tanaka, *J. Chem. Phys.*, 2000, **112**, 799–809.

42 H. Tanaka, *Phys. Rev. B: Condens. Matter Mater. Phys.*, 2002, **66**, 064202.

43 H. Tanaka, *Eur. Phys. J. E: Soft Matter Biol. Phys.*, 2012, **35**, 113.

44 R. Shi and H. Tanaka, *Proc. Natl. Acad. Sci. U. S. A.*, 2020, **117**, 26591–26599.

45 V. Holten, J. V. Sengers and M. A. Anisimov, *J. Phys. Chem. Ref. Data*, 2014, **43**, 043101.

46 P. H. Poole, F. Sciortino, T. Grande, H. E. Stanley and C. A. Angell, *Phys. Rev. Lett.*, 1994, **73**, 1632–1635.

47 F. Caupin and M. A. Anisimov, 2021, arXiv:2104.08117.

48 L. P. Singh, B. Issenmann and F. Caupin, *Proc. Natl. Acad. Sci. U. S. A.*, 2017, **114**, 4312–4317.

49 K. Ito, C. T. Moynihan and C. A. Angell, *Nature*, 1999, **398**, 492–495.

50 Y. Zhang, M. Lagi, E. Fratini, P. Baglioni, E. Mamontov and S.-H. Chen, *Phys. Rev. E: Stat., Nonlinear, Soft Matter Phys.*, 2009, **79**, 040201.

51 P. Gallo, M. Rovere and S. H. Chen, *J. Phys. Chem. Lett.*, 2010, **1**, 729–733.

52 Z. Wang, P. Le, K. Ito, J. B. Leão, M. Tyagi and S.-H. Chen, *J. Chem. Phys.*, 2015, **143**, 114508.

53 M. D. Marzio, G. Camisasca, M. Rovere and P. Gallo, *J. Chem. Phys.*, 2016, **144**, 074503.

54 A. Dehaoui, B. Issenmann and F. Caupin, *Proc. Natl. Acad. Sci. U. S. A.*, 2015, **112**, 12020–12025.

55 S.-H. Chen, F. Mallamace, C.-Y. Mou, M. Broccio, C. Corsaro, A. Faraone and L. Liu, *Proc. Natl. Acad. Sci. U. S. A.*, 2006, **103**, 12974–12978.

56 P. Kumar, *Proc. Natl. Acad. Sci. U. S. A.*, 2006, **103**, 12955–12956.

57 S. R. Becker, P. H. Poole and F. W. Starr, *Phys. Rev. Lett.*, 2006, **97**, 055901.

58 P. Kumar, S. V. Buldyrev, S. R. Becker, P. H. Poole, F. W. Starr and H. E. Stanley, *Proc. Natl. Acad. Sci. U. S. A.*, 2007, **104**, 9575–9579.

59 M. G. Mazza, N. Giovambattista, H. E. Stanley and F. W. Starr, *Phys. Rev. E: Stat., Nonlinear, Soft Matter Phys.*, 2007, **76**, 031203.

60 L. Xu, F. Mallamace, Z. Yan, F. W. Starr, S. V. Buldyrev and H. Eugene Stanley, *Nat. Phys.*, 2009, **5**, 565–569.

61 S. H. Chong, S. H. Chen and F. Mallamace, *J. Phys.: Condens. Matter*, 2009, **21**, 504101.

62 P. Montero de Hijes, E. Sanz, L. Joly, C. Valeriani and F. Caupin, *J. Chem. Phys.*, 2018, **149**, 094503.

63 N. Galamba, *J. Phys.: Condens. Matter*, 2016, **29**, 015101.

64 S. Dueby, V. Dubey and S. Daschakraborty, *J. Phys. Chem. B*, 2019, **123**, 7178–7189.

65 V. Dubey, S. Erimban, S. Indra and S. Daschakraborty, *J. Phys. Chem. B*, 2019, **123**, 10089–10099.

66 V. Dubey and S. Daschakraborty, *J. Phys. Chem. B*, 2020, **124**, 10398–10408.

67 S. Chandrasekhar, *Rev. Mod. Phys.*, 1943, **15**, 1–89.

68 S. Chandrasekhar, *Rev. Mod. Phys.*, 1949, **21**, 383–388.

69 A. Einstein and R. Fürth, *Investigations on the theory of Brownian movement*, Dover Publications, New York, N.Y., 1956.

70 D. S. Ray, 1999, arXiv preprint physics/9903033.

71 C. Goy, M. A. C. Potenza, S. Dedera, M. Tomut, E. Guillerm, A. Kalinin, K.-O. Voss, A. Schottelius, N. Petridis, A. Prosvetov, G. Tejeda, J. M. Fernández, C. Trautmann, F. Caupin, U. Glasmacher and R. E. Grisenti, *Phys. Rev. Lett.*, 2018, **120**, 015501.

72 D. Rosenfeld and W. L. Woodley, *Nature*, 2000, **405**, 440–442.

73 B. Riechers, F. Wittbracht, A. Hütten and T. Koop, *Phys. Chem. Chem. Phys.*, 2013, **15**, 5873–5887.

74 P. Taborek, *Phys. Rev. B: Condens. Matter Mater. Phys.*, 1985, **32**, 5902–5906.

75 D. E. Hare and C. M. Sorensen, *J. Chem. Phys.*, 1986, **84**, 5085–5089.

76 B. J. Mason, *Adv. Phys.*, 1958, **7**, 221–234.

77 H. Kanno, R. J. Speedy and C. A. Angell, *Science*, 1975, **189**, 880–881.

78 N. J. Hestand and J. L. Skinner, *J. Chem. Phys.*, 2018, **149**, 140901.

79 J. A. Sellberg, C. Huang, T. A. McQueen, N. D. Loh, H. Laksmono, D. Schlesinger, R. G. Sierra, D. Nordlund, C. Y. Hampton, D. Starodub, D. P. DePonte, M. Beye, C. Chen, A. V. Martin, A. Barty, K. T. Wikfeldt, T. M. Weiss, C. Caronna, J. Feldkamp, L. B. Skinner, M. M. Seibert, M. Messerschmidt, G. J. Williams, S. Boutet, L. G. M. Pettersson, M. J. Bogan and A. Nilsson, *Nature*, 2014, **510**, 381–384.

80 R. Bergman and J. Swenson, *Nature*, 2000, **403**, 283–286.

81 K. Koga, H. Tanaka and X. C. Zeng, *Nature*, 2000, **408**, 564–567.

82 B. Webber and J. Dore, *J. Phys.: Condens. Matter*, 2004, **16**, S5449–S5470.

83 J. Dore, *Chem. Phys.*, 2000, **258**, 327–347.

84 S. Cerveny, F. Mallamace, J. Swenson, M. Vogel and L. Xu, *Chem. Rev.*, 2016, **116**, 7608–7625.

85 L. Berthier, G. Biroli, J.-P. Bouchaud, L. Cipelletti, D. E. Masri, D. L'Hôte, F. Ladieu and M. Pierno, *Science*, 2005, **310**, 1797–1800.

86 F. H. Stillinger and J. A. Hodgdon, *Phys. Rev. E: Stat. Phys., Plasmas, Fluids, Relat. Interdiscip. Top.*, 1994, **50**, 2064–2068.

87 G. Tarjus and D. Kivelson, *J. Chem. Phys.*, 1995, **103**, 3071–3073.

88 E. R. Weeks, J. C. Crocker, A. C. Levitt, A. Schofield and D. A. Weitz, *Science*, 2000, **287**, 627–631.

89 K. L. Ngai, *Philos. Mag. B*, 1999, **79**, 1783–1797.

90 F. Bruni, R. Mancinelli and M. A. Ricci, *Phys. Chem. Chem. Phys.*, 2011, **13**, 19773–19779.

91 S. Cerveny, J. Colmenero and A. Alegria, *Phys. Rev. Lett.*, 2006, **97**, 189802.

92 M. Tyagi, A. Arbe, J. Colmenero, B. Frick and J. R. Stewart, *Macromolecules*, 2006, **39**, 3007–3018.

93 A. C. Genix, A. Arbe, F. Alvarez, J. Colmenero, W. Schweika and D. Richter, *Macromolecules*, 2006, **39**, 3947–3958.

94 J. Swenson, *Phys. Rev. Lett.*, 2006, **97**, 189801.

95 J. Swenson and J. Teixeira, *J. Chem. Phys.*, 2010, **132**, 014508.

96 S. Capaccioli, K. L. Ngai, S. Ancherbak, P. A. Rolla and N. Shinyashiki, *J. Non-Cryst. Solids*, 2011, **357**, 641–654.

97 W. Doster, S. Busch, A. M. Gaspar, M. S. Appavou, J. Wuttke and H. Scheer, *Phys. Rev. Lett.*, 2010, **104**, 098101.

98 S. Khodadadi, S. Pawlus and A. P. Sokolov, *J. Phys. Chem. B*, 2008, **112**, 14273–14280.

99 S. Khodadadi, S. Pawlus, J. H. Roh, V. G. Sakai, E. Mamontov and A. P. Sokolov, *J. Chem. Phys.*, 2008, **128**, 195106.

100 M. G. Mazza, K. Stokely, S. E. Pagnotta, F. Bruni, H. E. Stanley and G. Franzese, *Proc. Natl. Acad. Sci. U. S. A.*, 2011, **108**, 19873–19878.

101 B. Jana and B. Bagchi, *J. Phys. Chem. B*, 2009, **113**, 2221–2224.

102 B. Jana, R. S. Singh and B. Bagchi, *Phys. Chem. Chem. Phys.*, 2011, **13**, 16220–16226.

103 S. H. Glarum, *J. Chem. Phys.*, 1960, **33**, 1371–1375.

104 D. Laage and J. T. Hynes, *Science*, 2006, **311**, 832–835.

105 D. Laage and J. T. Hynes, *J. Phys. Chem. B*, 2008, **112**, 14230–14242.

106 L. E. Bove, S. Klotz, T. Strässle, M. Koza, J. Teixeira and A. M. Saitta, *Phys. Rev. Lett.*, 2013, **111**, 185901.

107 E. Guillaud, S. Merabia, D. de Ligny and L. Joly, *Phys. Chem. Chem. Phys.*, 2017, **19**, 2124–2130.

108 Z. Shi, P. G. Debenedetti and F. H. Stillinger, *J. Chem. Phys.*, 2013, **138**, 12A526.

109 W. S. Price, H. Ide and Y. Arata, *J. Phys. Chem. A*, 1999, **103**, 448–450.

110 J. Qvist, C. Mattea, E. P. Sunde and B. Halle, *J. Chem. Phys.*, 2012, **136**, 204505.

111 F. Fujara, B. Geil, H. Sillescu and G. Fleischer, *Z. Phys. B: Condens. Matter*, 1992, **88**, 195–204.

112 I. Chang, F. Fujara, B. Geil, G. Heuberger, T. Mangel and H. Sillescu, *J. Non-Cryst. Solids*, 1994, **172**, 248–255.

113 I. Chang and H. Sillescu, *J. Phys. Chem. B*, 1997, **101**, 8794–8801.

114 M. T. Cicerone and M. D. Ediger, *J. Chem. Phys.*, 1996, **104**, 7210–7218.

115 S. F. Swallen, P. A. Bonvallet, R. J. McMahon and M. D. Ediger, *Phys. Rev. Lett.*, 2003, **90**, 015901.

116 S. F. Swallen and M. D. Ediger, *Soft Matter*, 2011, **7**, 10339–10344.

117 M. D. Ediger, *Annu. Rev. Phys. Chem.*, 2000, **51**, 99–128.

118 M. Vedamuthu, S. Singh and G. W. Robinson, *J. Phys. Chem.*, 1994, **98**, 2222–2230.

119 T. Kawasaki and K. Kim, *Sci. Adv.*, 2017, **3**, e1700399.

120 T. Kawasaki and K. Kim, *J. Stat. Mech.: Theory Exp.*, 2019, **2019**, 084004.

121 J. L. Abascal and C. Vega, *J. Chem. Phys.*, 2005, **123**, 234505.

122 M. A. González and J. L. F. Abascal, *J. Chem. Phys.*, 2011, **135**, 224516.

123 V. Dubey, S. Dueby, S. Erimban and S. Daschakraborty, *J. Indian Chem. Soc.*, 2019, **96**, 741–751.

124 V. Dubey, N. Kumar and S. Daschakraborty, *J. Phys. Chem. B*, 2018, **122**, 7569–7583.

125 S. Indra and S. Daschakraborty, *Chem. Phys. Lett.*, 2017, **685**, 322–327.

126 S. Sastry, P. G. Debenedetti and F. H. Stillinger, *Nature*, 1998, **393**, 554–557.

127 A. Mukherjee, S. Bhattacharyya and B. Bagchi, *J. Chem. Phys.*, 2002, **116**, 4577–4586.

128 S. Bhattacharyya and B. Bagchi, *Phys. Rev. Lett.*, 2002, **89**, 025504.

129 M. T. Cicerone, Q. Zhong and M. Tyagi, *Phys. Rev. Lett.*, 2014, **113**, 117801.

130 R. Pastore, A. Coniglio and M. Pica Ciamarra, *Soft Matter*, 2014, **10**, 5724–5728.

131 M. P. Ciamarra, R. Pastore and A. Coniglio, *Soft Matter*, 2016, **12**, 358–366.

132 S. M. Bhattacharyya, B. Bagchi and P. G. Wolynes, *Proc. Natl. Acad. Sci. U. S. A.*, 2008, **105**, 16077–16082.

133 M. Goldstein, *J. Chem. Phys.*, 1969, **51**, 3728–3739.

134 M. D. Marzio, G. Camisasca, M. Rovere and P. Gallo, *J. Chem. Phys.*, 2017, **146**, 084502.

135 A. Rahman, *Phys. Rev.*, 1964, **136**, A405–A411.

136 T. Chen, B. Smit and A. T. Bell, *J. Chem. Phys.*, 2009, **131**, 246101.

137 P. J. Daivis and D. J. Evans, *J. Chem. Phys.*, 1994, **100**, 541–547.

138 M. Mondello and G. S. Grest, *J. Chem. Phys.*, 1997, **106**, 9327–9336.

139 F. Müller-Plathe, S. C. Rogers and W. F. van Gunsteren, *Chem. Phys. Lett.*, 1992, **199**, 237–243.

140 H. Takeuchi, *J. Chem. Phys.*, 1990, **93**, 2062–2067.

141 S. Bhattacharyya, A. Mukherjee and B. Bagchi, *J. Chem. Phys.*, 2002, **117**, 2741–2746.

142 E. Tocci, D. Hofmann, D. Paul, N. Russo and E. Drioli, *Polymer*, 2001, **42**, 521–533.

143 S. Acharya, M. K. Nandi, A. Mandal, S. Sarkar and S. M. Bhattacharyya, *J. Phys. Chem. B*, 2015, **119**, 11169–11175.

144 A. V. Anil Kumar and S. K. Bhatia, *J. Phys. Chem. B*, 2006, **110**, 3109–3113.

145 T. E. Raptis, V. E. Raptis and J. Samios, *J. Phys. Chem. B*, 2007, **111**, 13683–13693.

146 T. E. Raptis, V. E. Raptis and J. Samios, *Mol. Phys.*, 2012, **110**, 1171–1178.

147 J. C. Araque, S. K. Yadav, M. Shadec, M. Maroncelli and C. J. Margulis, *J. Phys. Chem. B*, 2015, **119**, 7015–7029.

148 M. S. Shell, P. G. Debenedetti and F. H. Stillinger, *J. Phys.: Condens. Matter*, 2005, **17**, S4035.

149 S. Sengupta and S. Karmakar, *J. Chem. Phys.*, 2014, **140**, 224505.

150 I.-C. Yeh and G. Hummer, *J. Phys. Chem. B*, 2004, **108**, 15873–15879.

151 S. Tazi, A. Boțan, M. Salanne, V. Marry, P. Turq and B. Rotenberg, *J. Phys.: Condens. Matter*, 2012, **24**, 284117.

152 R. Torre, P. Bartolini and R. Righini, *Nature*, 2004, **428**, 296–299.

153 A. Taschin, P. Bartolini, R. Eramo, R. Righini and R. Torre, *Nat. Commun.*, 2013, **4**, 1–8.

154 R. J. Speedy and C. A. Angell, *J. Chem. Phys.*, 1976, **65**, 851–858.

155 F. Mallamace, C. Branca, C. Corsaro, N. Leone, J. Spooren, S.-H. Chen and H. E. Stanley, *Proc. Natl. Acad. Sci. U. S. A.*, 2010, **107**, 22457–22462.

156 N. Brahms, *Generalized Nonlinear Non-analytic Chi-Square Fitting*, MATLAB Central File Exchange, 2021.

157 W. H. Press, S. A. Teukolsky, W. T. Vetterling and B. P. Flannery, *Numerical Recipes 3rd Edition: The Art of Scientific Computing*, Cambridge University Press, 2007.

158 D. W. Marquardt, *J. Soc. Ind. Appl. Math.*, 1963, **11**, 431–441.

159 K. R. Harris and P. J. Newitt, *J. Chem. Eng. Data*, 1997, **42**, 346–348.

160 C. Corsaro, E. Fazio and D. Mallamace, *J. Chem. Phys.*, 2019, **150**, 234506.

161 J. Simpson and H. Carr, *Phys. Rev.*, 1958, **111**, 1201.

162 C. Cho, J. Urquidi, S. Singh and G. W. Robinson, *J. Phys. Chem. B*, 1999, **103**, 1991–1994.

163 F. Kurata, T. W. Yergovich and G. W. Swift, *J. Chem. Eng. Data*, 1971, **16**, 222–226.

164 S. Mikhail and W. Kimel, *J. Chem. Eng. Data*, 1961, **6**, 533–537.

165 R. L. Hurle, A. J. Easteal and L. A. Woolf, *J. Chem. Soc., Faraday Trans. 1*, 1985, **81**, 769–779.

166 G. Guevara-Carrión, J. Vrabec and H. Hasse, *J. Chem. Phys.*, 2011, **134**, 074508.

167 N. Asahi and Y. Nakamura, *J. Chem. Phys.*, 1998, **109**, 9879–9887.

168 N. Karger, T. Vardag and H. D. Lüdemann, *J. Chem. Phys.*, 1990, **93**, 3437–3444.

169 C. Corsaro, R. Maisano, D. Mallamace and G. Dugo, *Phys. A*, 2013, **392**, 596–601.

170 F. Kurata, T. W. Yergovich and G. W. Swift, *J. Chem. Eng. Data*, 1971, **16**, 222–226.

171 S. Z. Mikhail and W. R. Kimel, *J. Chem. Eng. Data*, 1961, **6**, 533–537.

172 D. Bulone, C. Spinnato, F. Madonia and M. U. Palma, *J. Chem. Phys.*, 1989, **91**, 408–415.

173 H. Kubota, S. Tsuda, M. Murata, T. Yamamoto, Y. Tanaka and T. Makita, *Rev. Phys. Chem. Jpn.*, 1980, **49**, 59–69.

174 R. Rey, K. B. Møller and J. T. Hynes, *J. Phys. Chem. A*, 2002, **106**, 11993–11996.

175 C. P. Lawrence and J. L. Skinner, *J. Chem. Phys.*, 2003, **118**, 264–272.

176 A. Luzar and D. Chandler, *Nature*, 1996, **379**, 55.

177 J. D. Eaves, J. J. Loparo, C. J. Fecko, S. T. Roberts, A. Tokmakoff and P. L. Geissler, *Proc. Natl. Acad. Sci. U. S. A.*, 2005, **102**, 13019–13022.

178 N. Galamba, *J. Phys. Chem. B*, 2013, **117**, 2153–2159.

179 J. R. Errington and P. G. Debenedetti, *Nature*, 2001, **409**, 318–321.

180 P. L. Chau and A. J. Hardwick, *Mol. Phys.*, 1998, **93**, 511–518.

181 S. Chatterjee, P. G. Debenedetti, F. H. Stillinger and R. M. Lynden-Bell, *J. Chem. Phys.*, 2008, **128**, 124511.

182 S. Daschakraborty, *J. Chem. Phys.*, 2018, **148**, 134501.

183 R. Shi, J. Russo and H. Tanaka, *J. Chem. Phys.*, 2018, **149**, 224502.

184 B. P. Bhowmik, I. Tah and S. Karmakar, *Phys. Rev. E*, 2018, **98**, 022122.

185 T. Pal and R. Biswas, *J. Chem. Phys.*, 2014, **141**, 104501.

186 T. Pal and R. Biswas, *J. Phys. Chem. B*, 2015, **119**, 15683–15695.

187 S. Indra and R. Biswas, *J. Phys. Chem. B*, 2016, **120**, 11214–11228.

188 B. Bagchi, *Water in biological and chemical processes: from structure and dynamics to function*, Cambridge University Press 2013.

189 S. Roy, S. Banerjee, N. Biyani, B. Jana and B. Bagchi, *J. Phys. Chem. B*, 2011, **115**, 685–692.

190 M. K. Hazra and B. Bagchi, *J. Chem. Phys.*, 2018, **149**, 084501.

191 V. V. Chaban, *Phys. Chem. Chem. Phys.*, 2018, **20**, 23754–23761.

192 S. Kumar, S. Sarkar and B. Bagchi, *J. Chem. Phys.*, 2020, **152**, 164507.

193 S. Sarkar, S. Banerjee, S. Roy, R. Ghosh, P. Ray and B. Bagchi, *J. Chem. Sci.*, 2015, **127**, 49–59.

194 T. Pradhan, P. Ghoshal and R. Biswas, *J. Chem. Sci.*, 2008, **120**, 275–287.

195 S. Indra and R. Biswas, *J. Chem. Phys.*, 2015, **142**, 204501.

196 T. Pradhan, P. Ghoshal and R. Biswas, *J. Phys. Chem. A*, 2008, **112**, 915–924.

197 S. Indra, B. Guchhait and R. Biswas, *J. Chem. Phys.*, 2016, **144**, 124506.

198 S. Indra and R. Biswas, *Mol. Simul.*, 2015, **41**, 471–482.

199 S. Banerjee, J. Furtado and B. Bagchi, *J. Chem. Phys.*, 2014, **140**, 194502.

200 S. Banerjee, R. Ghosh and B. Bagchi, *J. Phys. Chem. B*, 2012, **116**, 3713–3722.

201 D. Banik, A. Roy, N. Kundu and N. Sarkar, *J. Phys. Chem. B*, 2015, **119**, 9905–9919.

202 R. Zangi and L. J. Kaufman, *Phys. Rev. E: Stat., Nonlinear, Soft Matter Phys.*, 2007, **75**, 051501.

203 E. Flenner and G. Szamel, *Phys. Rev. E: Stat., Nonlinear, Soft Matter Phys.*, 2005, **72**, 011205.

204 K. Kim and S. Saito, *Phys. Rev. E: Stat., Nonlinear, Soft Matter Phys.*, 2009, **79**, 060501.

205 K. Kim and S. Saito, *J. Chem. Phys.*, 2010, **133**, 044511.

206 K. Kim and S. Saito, *J. Phys. Soc. Jpn.*, 2010, **79**, 093601.

207 K. R. Harris, *J. Chem. Phys.*, 2009, **131**, 054503.

208 D. Jeong, M. Y. Choi, H. J. Kim and Y. Jung, *Phys. Chem. Chem. Phys.*, 2010, **12**, 2001–2010.

209 M. Sha, X. Ma, N. Li, F. Luo, G. Zhu and M. D. Fayer, *J. Chem. Phys.*, 2019, **151**, 154502.

210 T. Köddermann, R. Ludwig and D. Paschek, *ChemPhysChem*, 2008, **9**, 1851–1858.

211 K. R. Harris, *J. Phys. Chem. B*, 2010, **114**, 9572–9577.

212 S. K. Das, P. K. Sahu and M. Sarkar, *J. Phys. Chem. B*, 2013, **117**, 636–647.

213 N. Subba, K. Polok, P. Piatkowski, B. Ratajska-Gadomska, R. Biswas, W. Gadomski and P. Sen, *J. Phys. Chem. B*, 2019, **123**, 9212–9221.

214 R. Biswas, A. Das and H. Shirota, *J. Chem. Phys.*, 2014, **141**, 134506.

215 Y. Wang, W. Chen, Q. Zhao, G. Jin, Z. Xue, Y. Wang and T. Mu, *Phys. Chem. Chem. Phys.*, 2020, **22**, 25760–25768.

216 B. B. Hansen, S. Spittle, B. Chen, D. Poe, Y. Zhang, J. M. Klein, A. Horton, L. Adhikari, T. Zelovich, B. W. Doherty, B. Gurkan, E. J. Maginn, A. Ragauskas, M. Dadmun, T. A. Zawodzinski, G. A. Baker, M. E. Tuckerman, R. F. Savinell and J. R. Sangoro, *Chem. Rev.*, 2021, **121**, 1232–1285.

217 A. Maity, S. Sarkar, L. Theeyancheri and R. Chakrabarti, *ChemPhysChem*, 2020, **21**, 552–567.

218 S. Wei, Z. Evenson, M. Stolpe, P. Lucas and C. A. Angell, *Sci. Adv.*, 2018, **4**, eaat8632.

219 G. C. Sosso, J. Colombo, J. Behler, E. Del Gado and M. Bernasconi, *J. Phys. Chem. B*, 2014, **118**, 13621–13628.

220 S. Wei, C. Persch, M. Stolpe, Z. Evenson, G. Coleman, P. Lucas and M. Wuttig, *Acta Mater.*, 2020, **195**, 491–500.

221 G. C. Sosso, J. Behler and M. Bernasconi, *Phys. Status Solidi B*, 2012, **249**, 1880–1885.

222 N. Ohtori, S. Miyamoto and Y. Ishii, *Phys. Rev. E*, 2017, **95**, 052122.

223 S. Pan, Z. W. Wu, W. H. Wang, M. Z. Li and L. Xu, *Sci. Rep.*, 2017, **7**, 39938.

224 S. Sengupta, S. Karmakar, C. Dasgupta and S. Sastry, *J. Chem. Phys.*, 2013, **138**, 12A548.

225 M. Sharma and S. Yashonath, *J. Phys. Chem. B*, 2006, **110**, 17207–17211.

226 M. K. Nandi and S. Maitra Bhattacharyya, *J. Phys.: Condens. Matter*, 2019, **32**, 064001.

227 A. D. S. Parmar, S. Sengupta and S. Sastry, *Phys. Rev. Lett.*, 2017, **119**, 056001.

228 L. Costigliola, D. M. Heyes, T. B. Schröder and J. C. Dyre, *J. Chem. Phys.*, 2019, **150**, 021101.

229 A. Das and S. M. Ali, *AIP Adv.*, 2020, **10**, 045327.

230 T. C. Chan, H. T. Li and K. Y. Li, *J. Phys. Chem. B*, 2015, **119**, 15718–15728.

231 P. Kumar, L. Theeyancheri, S. Chaki and R. Chakrabarti, *Soft Matter*, 2019, **15**, 8992–9002.

232 S. Chaki and R. Chakrabarti, *Soft Matter*, 2020, **16**, 7103–7115.

233 J. Świergiel, L. Bouteiller and J. Jadżyn, *Soft Matter*, 2014, **10**, 8457–8463.

234 B. Carroll, V. Bocharova, J.-M. Y. Carrillo, A. Kisliuk, S. Cheng, U. Yamamoto, K. S. Schweizer, B. G. Sumpter and A. P. Sokolov, *Macromolecules*, 2018, **51**, 2268–2275.

235 Y. Jung, J. P. Garrahan and D. Chandler, *J. Chem. Phys.*, 2005, **123**, 084509.

236 N. Samanta and R. Chakrabarti, *Soft Matter*, 2016, **12**, 8554–8563.

237 A. Bhattacharyay, *J. Phys. A: Math. Theor.*, 2020, **53**, 075002.

238 L. P. Faucheux and A. J. Libchaber, *Phys. Rev. E: Stat. Phys., Plasmas, Fluids, Relat. Interdiscip. Top.*, 1994, **49**, 5158–5163.

239 P. Lançon, G. Batrouni, L. Lobry and N. Ostrowsky, *Europhys. Lett.*, 2001, **54**, 28–34.

240 G. Volpe, L. Helden, T. Brettschneider, J. Wehr and C. Bechinger, *Phys. Rev. Lett.*, 2010, **104**, 170602.

241 M. Wolfson, C. Liepold, B. Lin and S. A. Rice, *J. Chem. Phys.*, 2018, **148**, 194901.

242 A. G. Cherstvy, A. V. Chechkin and R. Metzler, *New J. Phys.*, 2013, **15**, 083039.

243 T. Apajalahti, P. Niemelä, P. N. Govindan, M. S. Miettinen, E. Salonen, S.-J. Marrink and I. Vattulainen, *Faraday Discuss.*, 2010, **144**, 411–430.

244 S. Chiantia, J. Ries, N. Kahya and P. Schwille, *ChemPhysChem*, 2006, **7**, 2409–2418.

245 T. Fujiwara, K. Ritchie, H. Murakoshi, K. Jacobson and A. Kusumi, *J. Cell Biol.*, 2002, **157**, 1071–1082.

246 G. de Wit, J. S. H. Danial, P. Kukura and M. I. Wallace, *Proc. Natl. Acad. Sci. U. S. A.*, 2015, **112**, 12299–12303.

247 J.-H. Jeon, H. M.-S. Monne, M. Javanainen and R. Metzler, *Phys. Rev. Lett.*, 2012, **109**, 188103.

248 E. Sezgin, I. Levental, S. Mayor and C. Eggeling, *Nat. Rev. Mol. Cell Biol.*, 2017, **18**, 361–374.

249 R. Regmi, P. M. Winkler, V. Flauraud, K. J. E. Borgman, C. Manzo, J. Brugger, H. Rigneault, J. Wenger and M. F. García-Parajo, *Nano Lett.*, 2017, **17**, 6295–6302.

250 N. K. Sarangi, K. G. Ayappa and J. K. Basu, *Sci. Rep.*, 2017, **7**, 11173.

251 Y.-H. Liao, C.-H. Lin, C.-Y. Cheng, W. C. Wong, J.-Y. Juo and C.-L. Hsieh, *ACS Nano*, 2019, **13**, 10918–10928.

252 G. de Wit, D. Albrecht, H. Ewers and P. Kukura, *Biophys. J.*, 2018, **114**, 2945–2950.

253 E. Yamamoto, T. Akimoto, A. Mitsutake and R. Metzler, *Phys. Rev. Lett.*, 2021, **126**, 128101.

254 D. Laage, T. Elsaesser and J. T. Hynes, *Chem. Rev.*, 2017, **117**, 10694–10725.

255 B. Bagchi, *Proc. Natl. Acad. Sci. U. S. A.*, 2016, **113**, 8355–8357.

256 N. Nandi and B. Bagchi, *J. Phys. Chem. B*, 1997, **101**, 10954–10961.

257 S. K. Pal, J. Peon, B. Bagchi and A. H. Zewail, *J. Phys. Chem. B*, 2002, **106**, 12376–12395.

258 A. L. Agapov, A. I. Kolesnikov, V. N. Novikov, R. Richert and A. P. Sokolov, *Phys. Rev. E: Stat., Nonlinear, Soft Matter Phys.*, 2015, **91**, 022312.

259 A. Wallqvist and B. J. Berne, *Chem. Phys. Lett.*, 1985, **117**, 214–219.

260 S. Habershon, T. E. Markland and D. E. Manolopoulos, *J. Chem. Phys.*, 2009, **131**, 024501.

261 J. Lobaugh and G. A. Voth, *J. Chem. Phys.*, 1997, **106**, 2400–2410.

262 L. H. d. l. Peña and P. G. Kusalik, *J. Chem. Phys.*, 2004, **121**, 5992–6002.

263 T. F. M. Iii and D. E. Manolopoulos, *J. Chem. Phys.*, 2005, **123**, 154504.

264 L. H. d. l. Peña and P. G. Kusalik, *J. Chem. Phys.*, 2006, **125**, 054512.

265 F. Paesani, W. Zhang, D. A. Case, T. E. Cheatham III and G. A. Voth, *J. Chem. Phys.*, 2006, **125**, 184507.

266 F. Paesani, S. Iuchi and G. A. Voth, *J. Chem. Phys.*, 2007, **127**, 074506.

267 B. Guillot and Y. Guissani, *J. Chem. Phys.*, 1998, **108**, 10162–10174.

268 J. A. Poulsen, G. Nyman and P. J. Rossky, *Proc. Natl. Acad. Sci. U. S. A.*, 2005, **102**, 6709–6714.